Supplementary Information (SI) for Physical Chemistry Chemical Physics.
This journal is © the Owner Societies 2024

A Water-Responsive Calix[4]Resorcinarene System: Self-Assembly and Fluorescence Modulation

María Virginia Sosa[1], Kashif Hussain[2], Eduardo D. Prieto[1,4], Tatiana Da Ros[3], M. Raza Shah[2], Fernando S. García Einschlag[1]* and Ezequiel Wolcan[1]*

[1] Instituto de Investigaciones Fisicoquímicas Teóricas y Aplicadas (INIFTA, UNLP, CCT La Plata-CONICET), Diag. 113 y 64, Sucursal 4, C.C. 16, (B1906ZAA) La Plata, Argentina.

[2] H.E.J. Research Institute of Chemistry, International Center for Chemical and Biological Sciences, University of Karachi, 75270, Karachi, Pakistan

[3] INSTM, Department of Chemical and Pharmaceutical Sciences, University of Trieste, Via L. Giorgieri 1, 34127, Trieste, Italy

[4] Departamento de Cs. Biológicas, Facultad de Ciencias Exactas (UNLP), Instituto Ciencias de la Salud, Universidad Nacional Arturo Jauretche (UNAJ), Argentina

*Fernando S. Garcia Einschlag, fgarciae@quimica.unlp.edu.ar

*Ezequiel Wolcan, ewolcan@inifta.unlp.edu.ar

TABLE OF CONTENTS

MATERIALS AND METHODS

1. Materials and Instrumentation

All the necessary chemicals, including 4-hydroxybenzaldehyde, potassium carbonate (K_2CO_3), resorcinol, 1-hexadecanoyl chloride, and acetone, were obtained from Wako Pure Chemical Industries in Osaka, Japan. Distilled water was used to prepare all the solutions, and analytical grade solvents were used in this research without any further purification. Commercial-grade solvents (n-hexane, ethyl acetate, dichloromethane) were employed to purify the compounds through silica gel chromatography after distillation. UV-visible analysis was performed using a Cary-60 spectrophotometer, while ^{1}H-NMR spectroscopy was carried out using a Bruker AVANCE III spectrometer. Molecular mass was determined by ESI-MS (Bruker Compass Data Analysis 4.2).

2. Atomic Force Microscopy

The formation of **C2** macrocycle aggregates from neat THF or TFH/H_2O solutions was observed using Atomic Force Microscopy (AFM). The concentration of the macrocycle was kept at 4×10^{-8} M in all experiments, and a 10 ml sample was spotted onto freshly cleaved muscovite mica in a stepwise manner. The sample was then dried under N_2. All images were captured in ambient conditions with a MultiMode Scanning Probe Microscope (Veeco, Santa Barbara, CA, USA) equipped with a Nanoscope V controller (Veeco, Santa Barbara, CA). The measurements were obtained in tapping mode using probes doped with silicon nitride (RTESP, Veeco) with a tip radius of 8-12 nm, 271-311 kHz, and a force constant of 20-80 N/m. The typical scan rates ranged from 1-1.5 Hz.

3. Steady-state and time-resolved emission experiments

In this study, fluorescence measurements were conducted using single-photon-counting equipment, FL3 TCSPC-SP (Horiba Jobin Yvon), at room temperature. The emission spectra were adjusted for source intensity (lamp and grating) using standard correction curves. Fluorescence quantum yields were measured using an Edinburgh Spectrofluorometer FS5 with SC-30 integrating sphere cassette. For time-resolved fluorescence experiments, a NanoLED excitation source (maxima at 295 nm) was used. The emitted photons were detected by a TBX-04 detector, which was connected to a TBX-PS power supply and counted by a FluoroHub-B module. The DataStation measurement control software application was used to control the module. The counting time window for the measurements reported in this study was 0 - 200 ns. The decay curve was measured at 320, 330, and 340 nm for a given solution. Lifetime analysis was performed using the commercial DAS6 Fluorescence Decay Analysis software. The quality of the fit was assessed by minimizing the reduced chi-squared function (χ^2) and visual inspection of the weighted residuals and their autocorrelation. A fit calculation (up to 2 exponentials) was performed on the separate 320, 330, and 340 nm fluorescence decay curves. For samples with lifetimes in the ns order, an instrument response function calibration (IRF) was performed using a diluted Ludox® dispersion.

4. Dynamic Light Scattering

The size of the particles of **C2** was measured using Dynamic Light Scattering (DLS) in neat THF, as well as in THF/H_2O mixtures containing different percentages of water (67/33, 53/47, 33/67, 18/82 and 5/95 v/v) at 25°C. The concentration range for DLS measurements of **C2** was between 0.5mM and 1.5mM. The Zetasizer Nano equipment (Nano ZSizer-ZEN3600, Malvern, UK) was used for the measurements.

5. Synthesis and characterization of macrocycle compounds

5.1. Synthesis and characterization of C2

The compound **C2,** (2, 4, 6, 8-tetrakis (4-octadecyloxy)-3-methoxyphenyl)-1, 3, 5, 7(1, 3)-tetrabenzenacyclooctaphan-1^4, 1^6, 3^4, 3^6, 5^4, 5^6, 7^4, 7^6-octaol), was synthesized through a reaction between compound **(a)** and resorcinol (see **Scheme S1**). Compound **(a)** was prepared by reacting 4-hydroxy-3-methoxybenzaldehyde with 1-bromooctadecane in presence of K_2CO_3 in acetone at 80^o C involving a bimolecular nucleophilic substitution reaction. The progress of the reaction was monitored using the TLC technique with the solvent system consisting of n-hexane and ethyl acetate (9:1, v/v). After the reaction was completed, it was stopped and cooled at room temperature. The salt-added water was removed, and the resulting mixture was extracted with ethyl acetate. The extract was then purified through column chromatography using n-hexane and ethyl acetate in a 98:2 ratio (v/v). EI-MS, ^{1}H-NMR and FT-IR spectroscopy. EI-MS technique was used to determine the molecular mass (**Figure S1**) which observed at 404.4 *m/z* in agreement with the molecular formula $C_{26}H_{44}O_3$. Further characterization was performed by ^{1}H-NMR, FTIR, and melting point. The ^{1}H-NMR of **(b)** was performed at 400 MHz in $CDCl_3$ (**Figure S2**). A singlet of methyl proton at δ 0.85 of 3H proton, a multiplet CH_2 with 30H at δ 1.23, a singlet with 2H of methylene at δ 1.85, at δ 3.90, a singlet of OCH_3 for 3H proton, a singlet of CH_2 with 2H at δ 4.07, a doublet of benzene at δ 6.92 with 1H proton) giving a coupling constant 8.0 Hz, a doublet of CH of aromaticing at δ 7.38 for 2H with coupling constant 8.0 Hz. FT-IR (KBr, cm^{-1}): 2915.7 (C-H, CH_3), 2849.1 (C-H, CH_2), 1677.3 (aromatic aldehyde, CHO), 1590.9 (C=C, aromatic group), 1270.8 (ether, -O-CH_3, -O-CH_2). Yield: 1825 mg, 90.3 %, M.P.: 72.1 – 75.3 °C.

The compound **C2** was obtained by cyclizing compound **(b)** and resorcinol in the presence of sulfuric acid as a catalyst and acetic acid as a solvent. The reaction mixture was heated at 80ºC for 24 hrs. A brown precipitate was formed, which was filtered, and various spectroscopic techniques were utilized for the characterization of the synthesized compound.

The ^{1}H-NMR were performed at 400 MHz in pyridine (**Figure S3**) and a triplet of methyl proton at δ 0.83 with coupling constant 8.0 Hz with 12H, a multiplet of 112H at δ 1.25 of methylene group, a triplet of methylene group at δ 1.50 appeared with at 8H with coupling constants 8.0 Hz, at δ 1.87, triplet of methylene proton appeared with 8H with coupling constants 6.7 Hz, a singlet of methoxy proton appeared at δ 3.68 with 12H, 4.05 (t, 8H, CH2, J = 7.6 Hz), a singlet of 4H of CH of cycle appeared at δ 6.75, a singlet of 4H of ArCH appeared at δ 6.85, a doublet of 4H of ArCH with coupling constant 12 Hz appeared at δ 6.97, a triplet of 8H of ArCH with coupling constant 16 Hz appeared at δ 7.13, a singlet of 8H of hydroxyl appeared at δ 10.48. FT-IR (KBr, cm-1): 3392.0 (OH), 2920.5 (CH_3), 2851.8 (CH_2), 1609.6 (aldehyde), 1509.3 (aromatic group), 1245.9 cm^{-1} (ether group). Yield: 1780 mg, 89.6%. M.P. 176-180ºC.

The ESI-HR-MS technique was utilized to determine the molecular mass (**Figure S4-a**), and the EA demonstrated the coprecipitation of acetic acid with the target compound.

ESI-HR-MS (MeOH, $C_{128}H_{192}O_{16}H^+$, M+H, m/z): calcd. for $C_{128}H_{192}O_{16}H^+ = 1986.4254$, found $C_{128}H_{192}O_{16}H^+ = 1986.4283$.

EA. Calculated for $C_{128}H_{192}O_{16} \cdot CH_3CO_2H$: C = 76.28%, H = 9.65 %, N = 0 %. Found: C = 76.61, H = 9.63, N = 0 %.

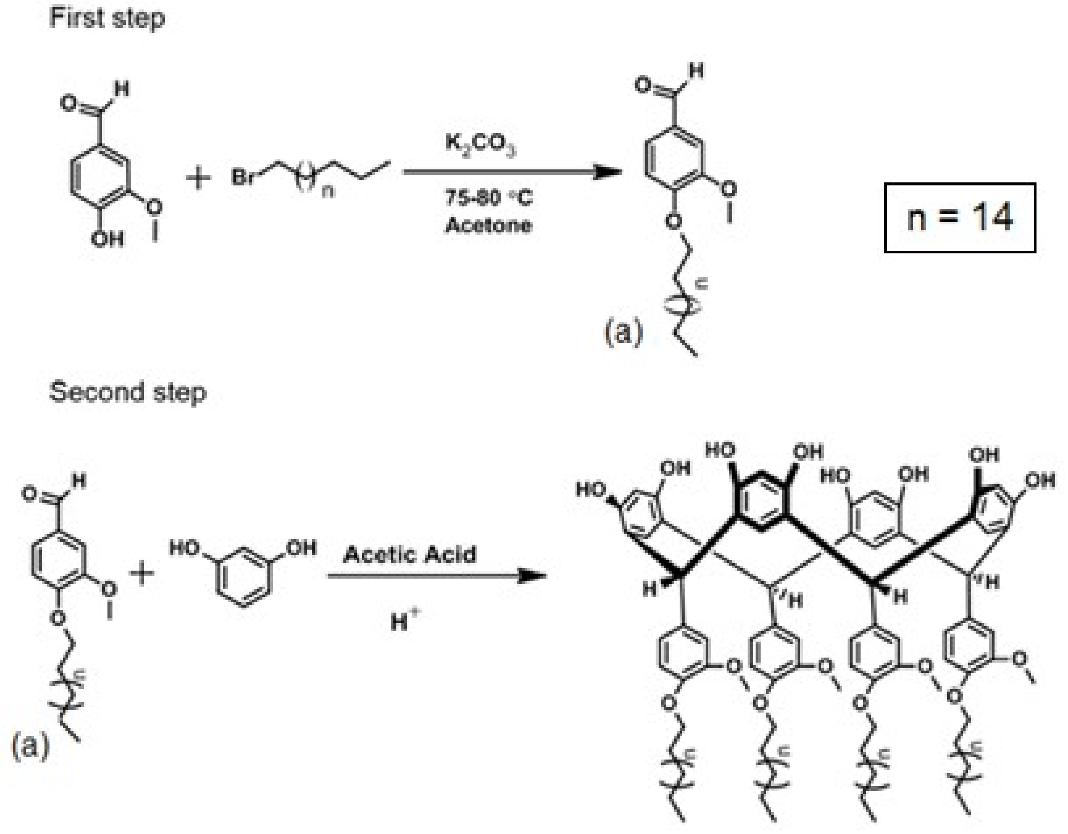

Scheme S1. The schematic illustration shows the synthesis of a functionalized calix4resorcinarene macrocycle through a two-step reaction.

5.2. ESI-HR-MS and EA characterization of C1

The ESI-HR-MS technique was utilized to determine the molecular mass (**Figure S4-b**), and the EA demonstrated the coprecipitation of acetic acid with the target compound.

ESI-HR-MS (MeOH, $C_{120}H_{176}O_{16}H^+$, M+H, m/z): calcd. for $C_{120}H_{176}O_{16}H^+ = 1874.3006$, found $C_{120}H_{176}O_{16}H^+ = 1874.3031$.

EA. Calculated for $C_{120}H_{176}O_{16} \cdot 4\ CH_3CO_2H$: C = 72.69%, H = 9.15 %, N = 0 %. Found: C = 72.29, H = 9.22, N = 0 %.

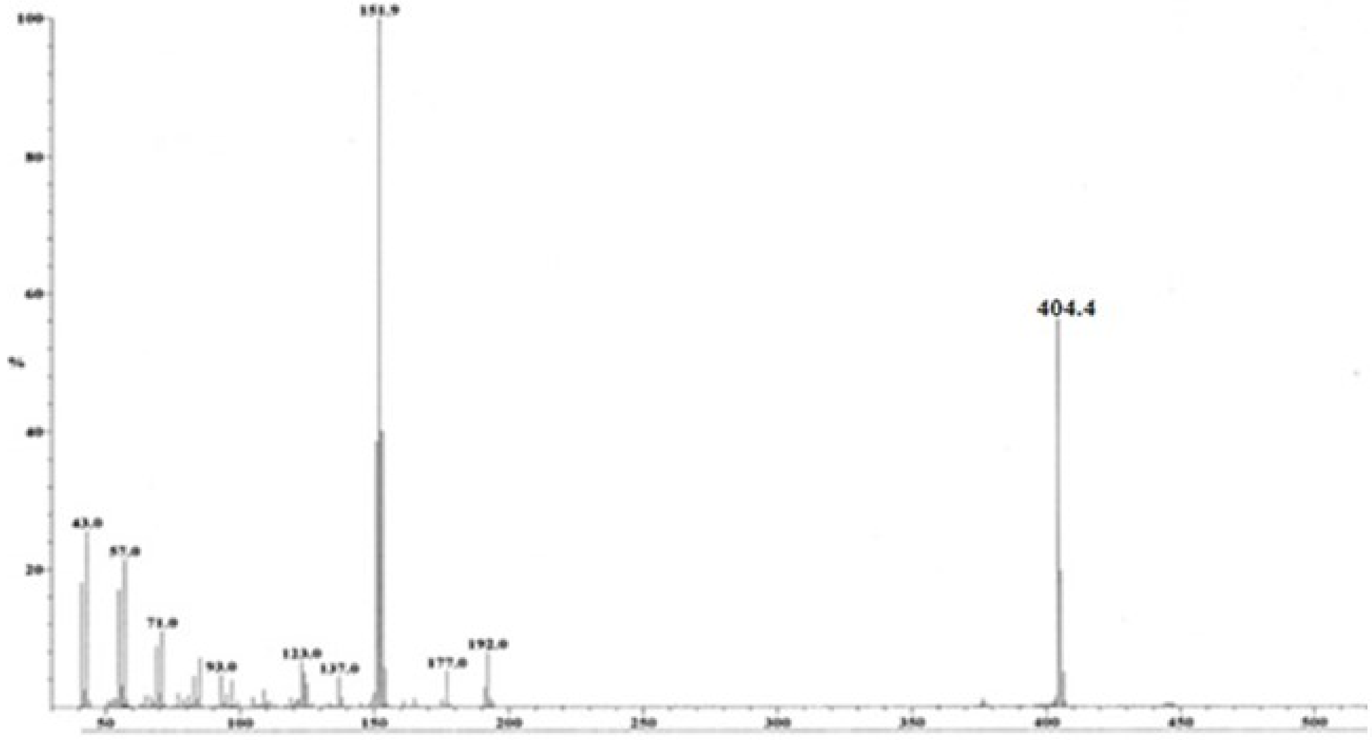

Figure S1. ESI-MS spectra of compound **(a)**

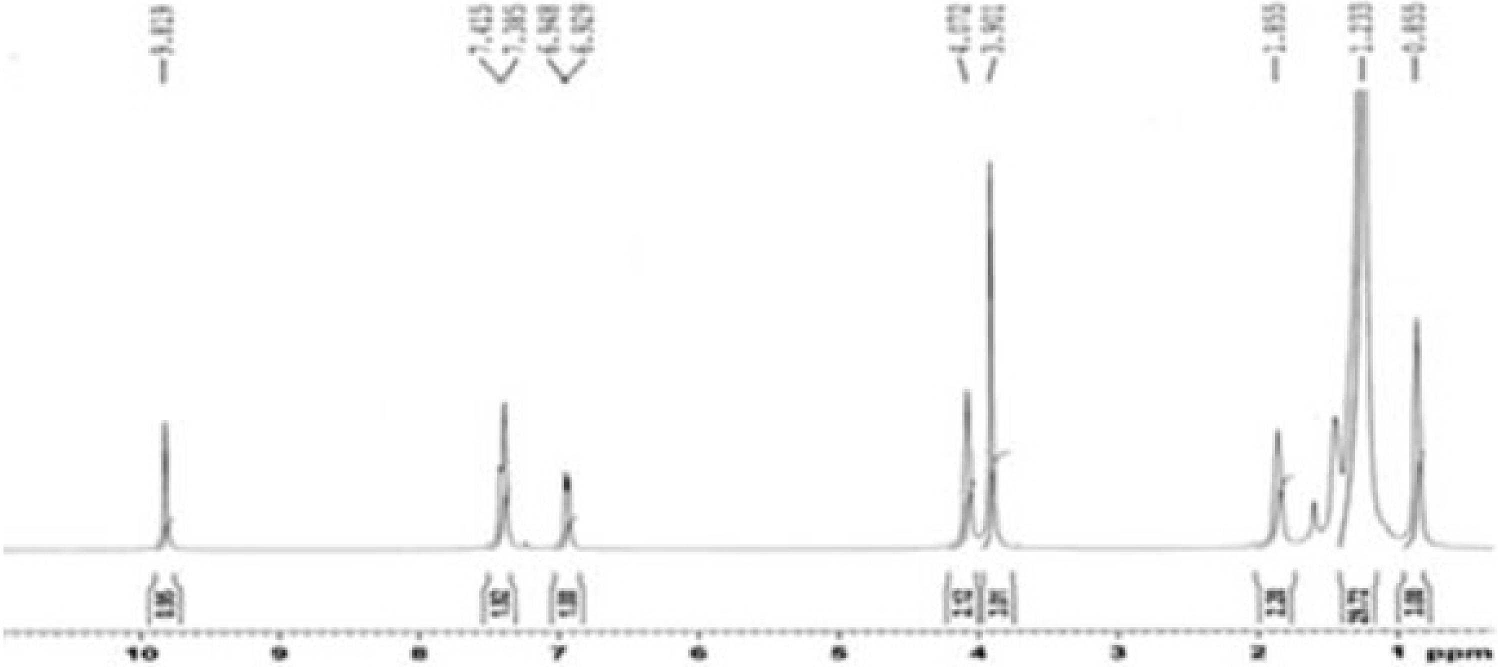

Figure S2. ^{1}H NMR spectra of compound **(a)**

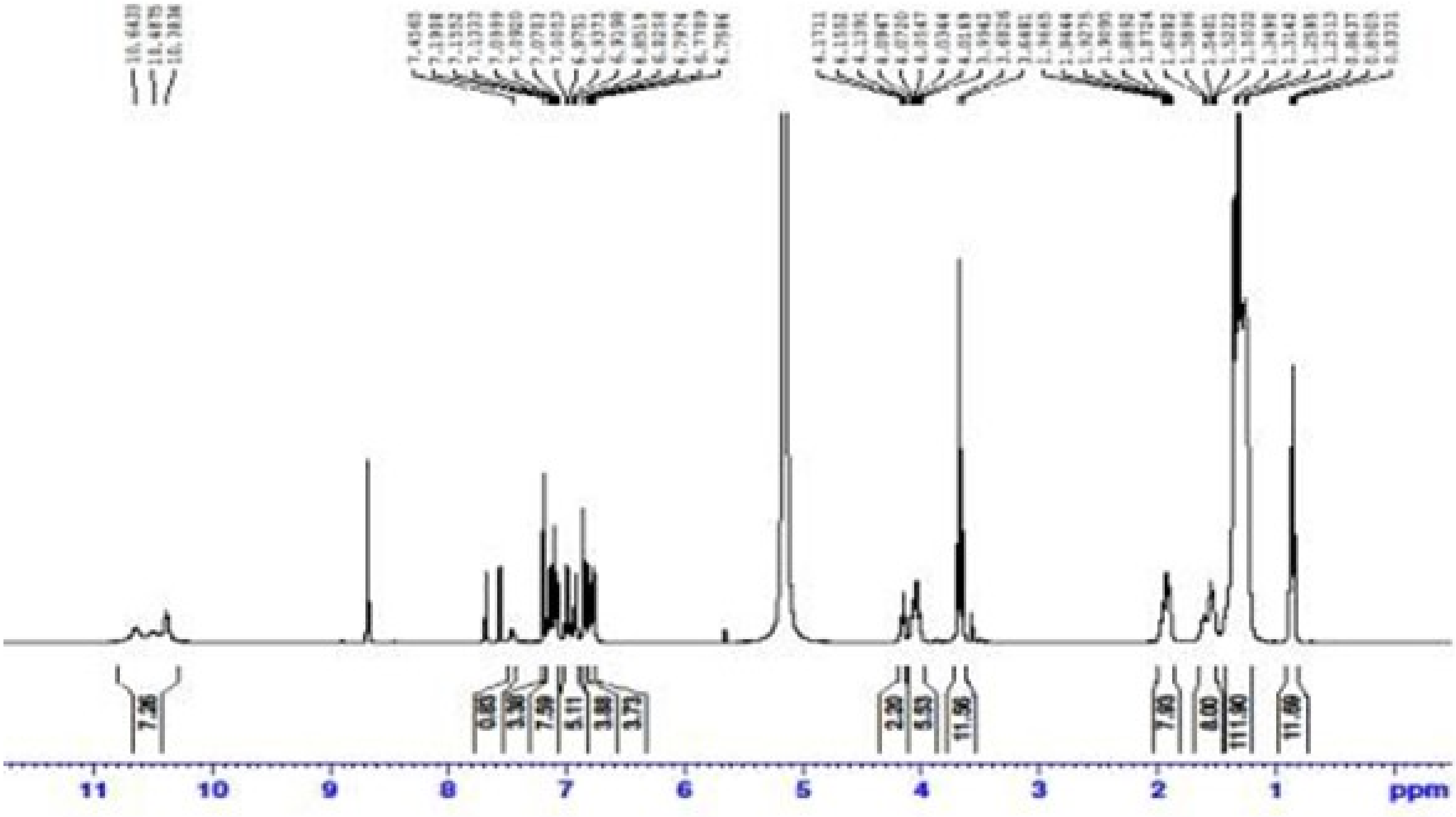

Figure S3. ^{1}H NMR spectra of compound **C2**

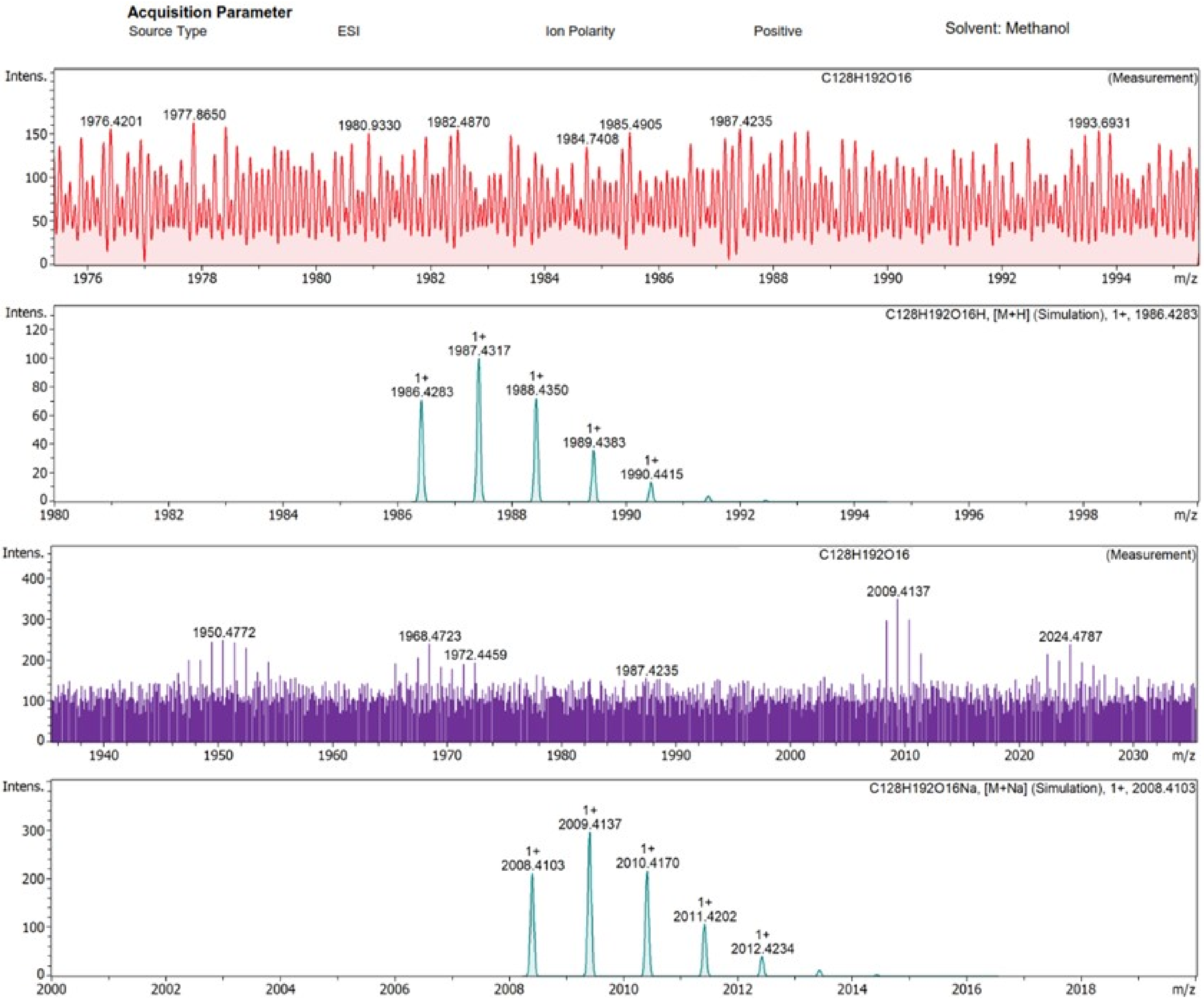
Acquisition Parameter

Source Type ESI

Ion Polarity Positive

Solvent: Methanol

Figure S4-a. ESI-HR-MS spectra of compound **C2**

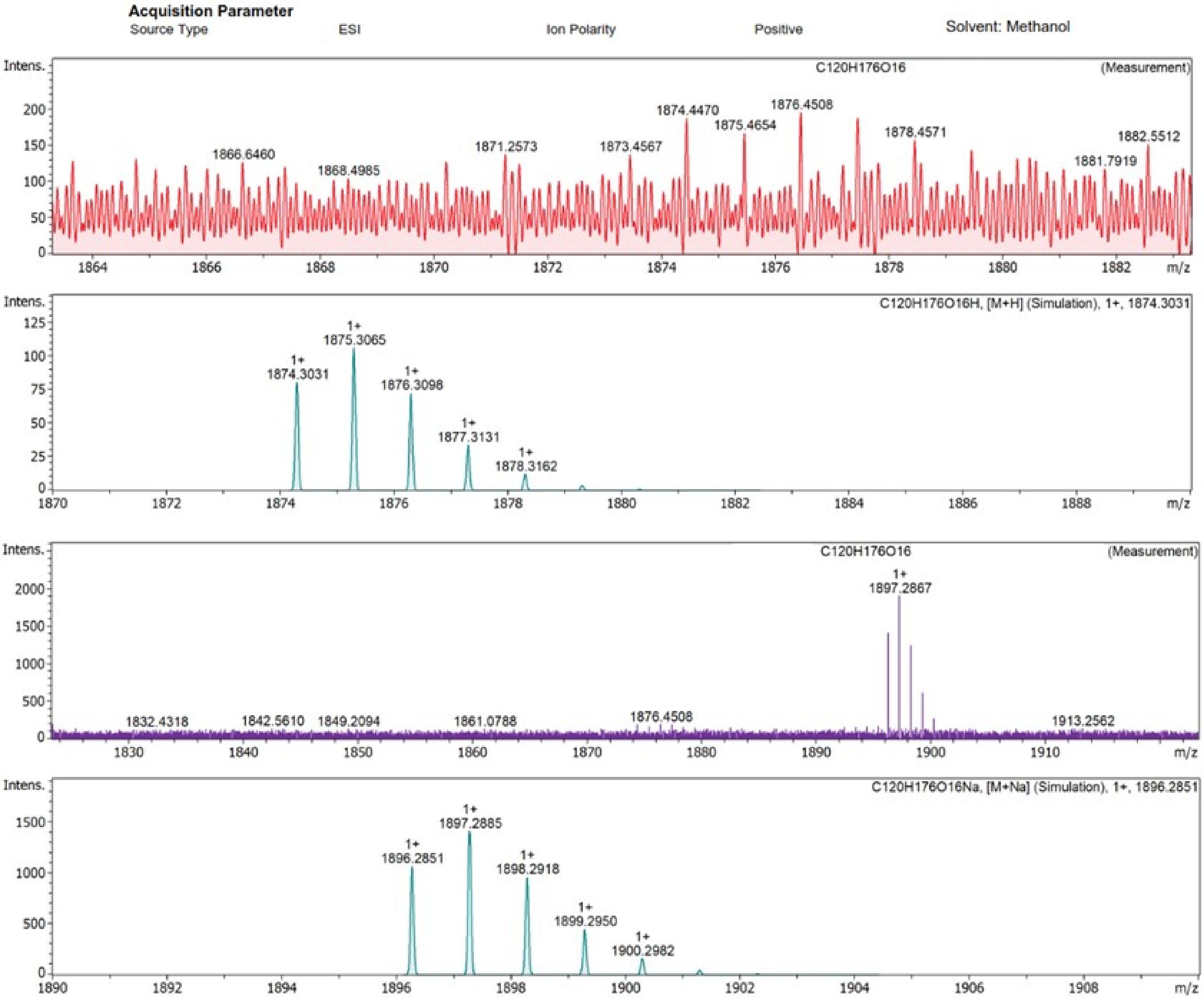
Acquisition Parameter
Source Type ESI
Ion Polarity Positive
Solvent: Methanol

Figure S4-b. ESI-HR-MS spectra of compound **C1**

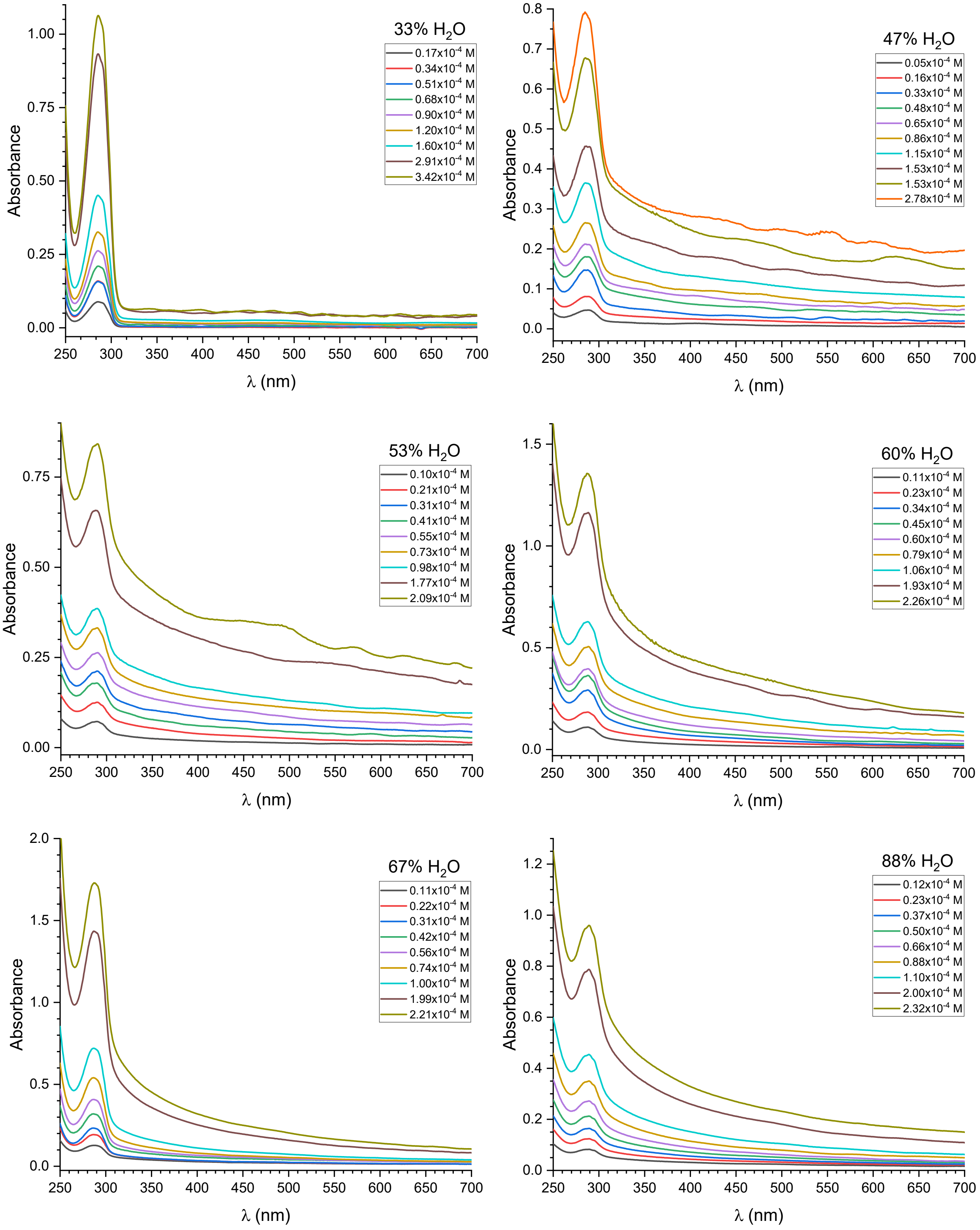

Figure S5. Absorption spectra of **C2** at several concentrations in THF/H_2O solutions at 33, 47, 53, 60, 67 and 88 % of H_2O

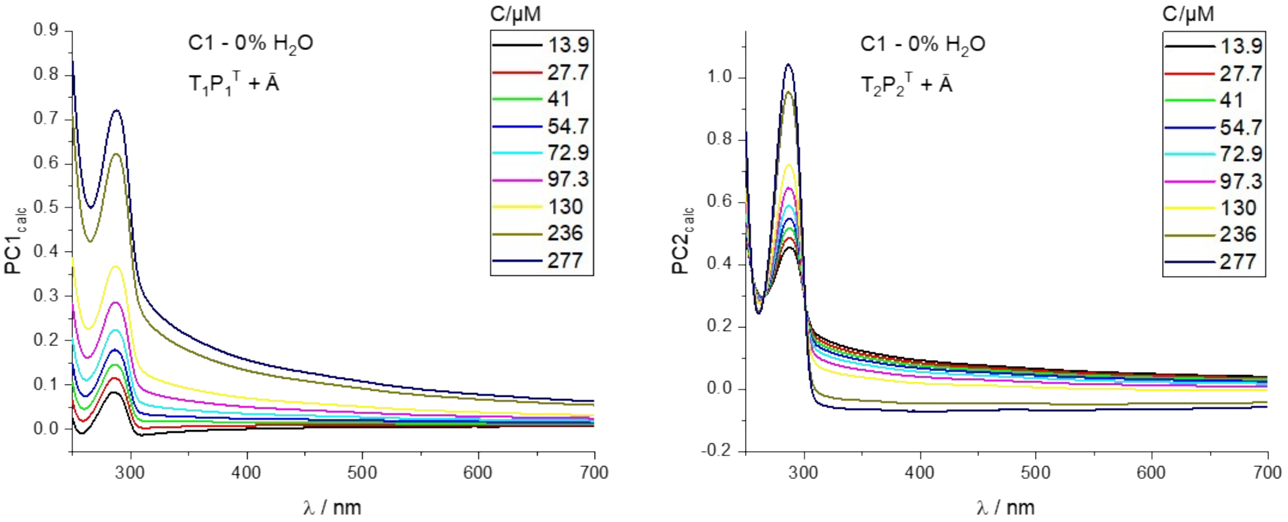

Figure S6: Core data structure for **C1** at 0% H_2O content

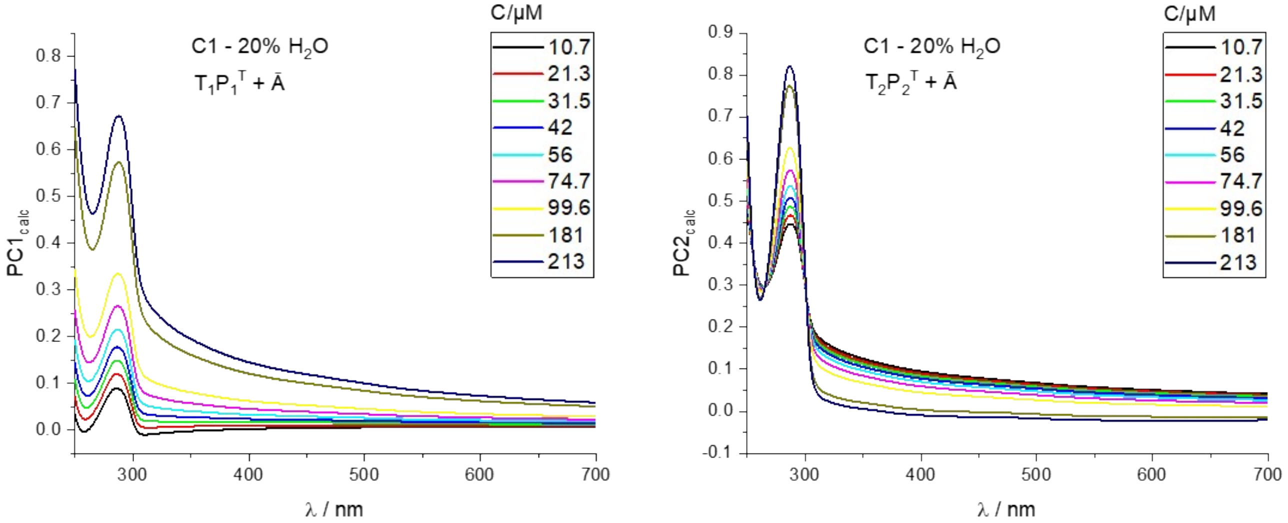

Figure S7: Core data structure for **C1** at 20% H_2O content

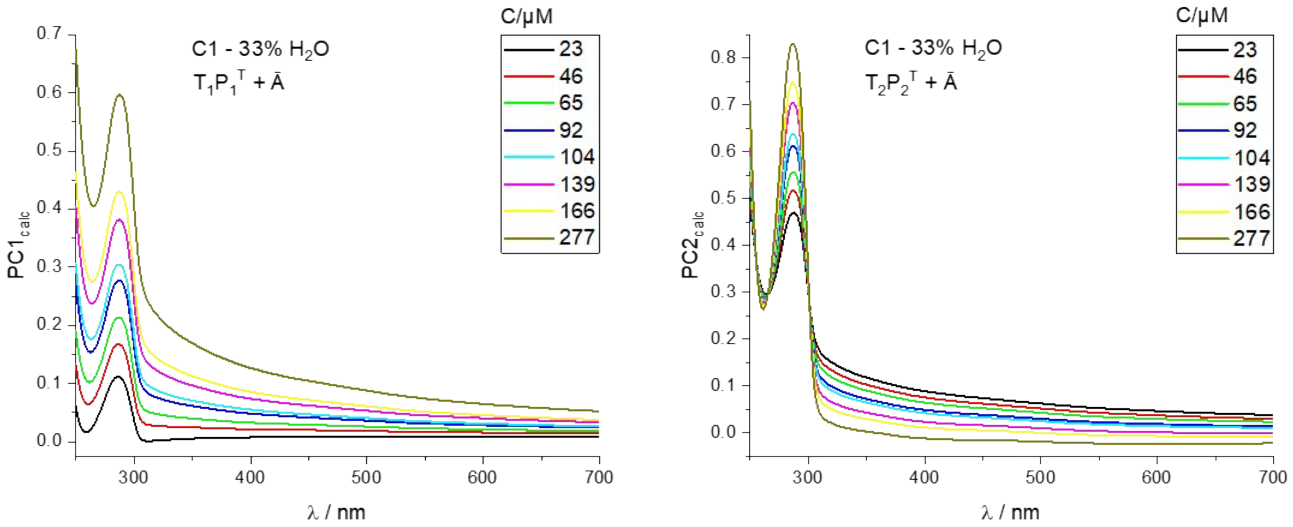

Figure S8: Core data structure for **C1** at 33% H_2O content

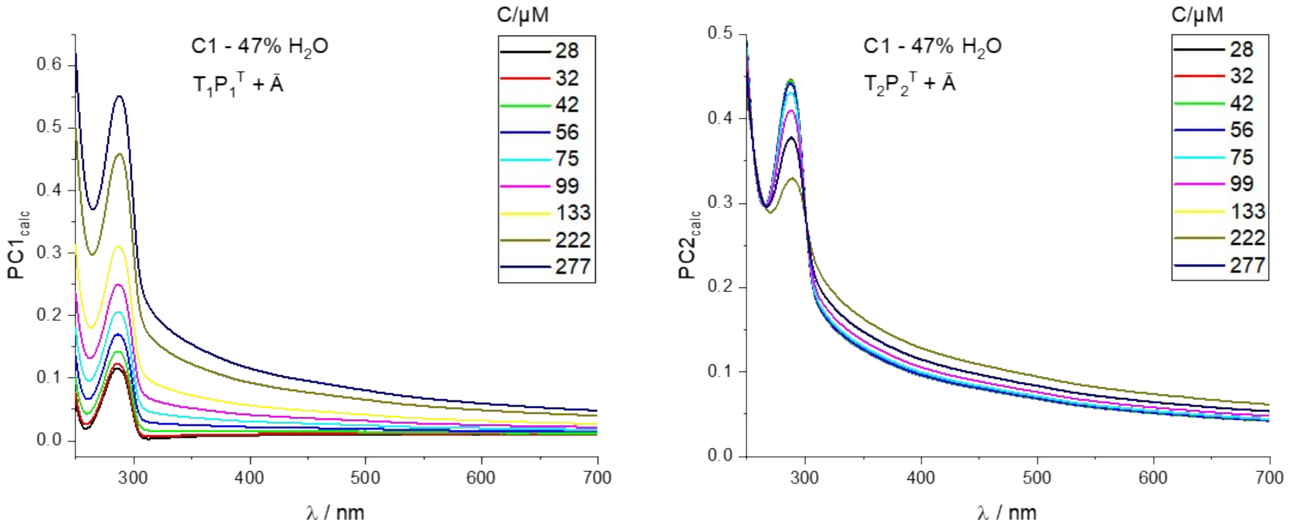

Figure S9: Core data structure for **C1** at 47% H_2O content

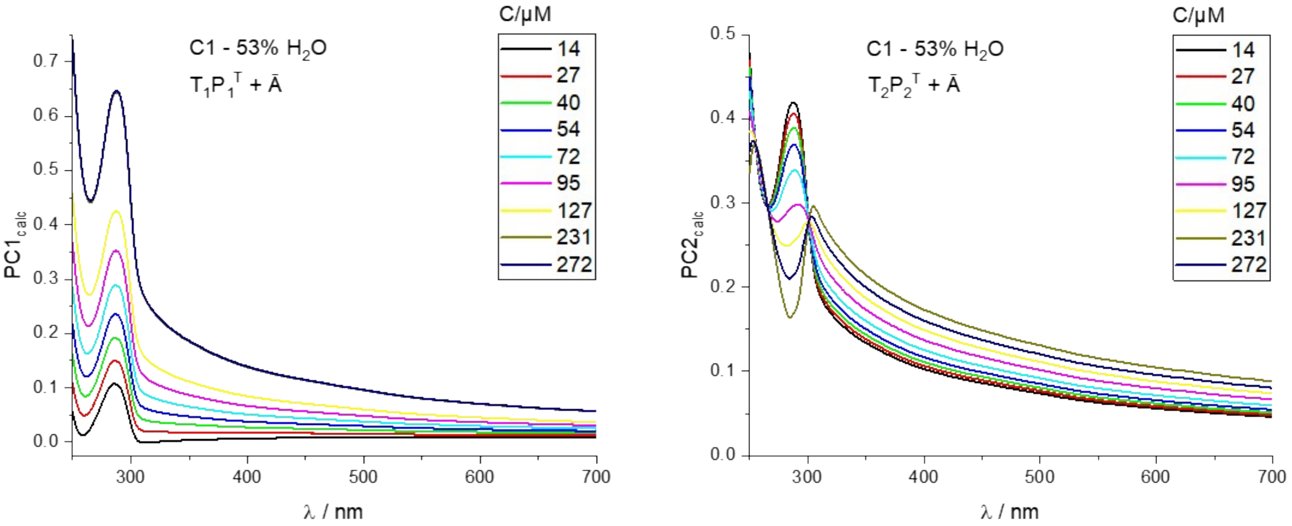

Figure S10: Core data structure for **C1** at 53% H_2O content

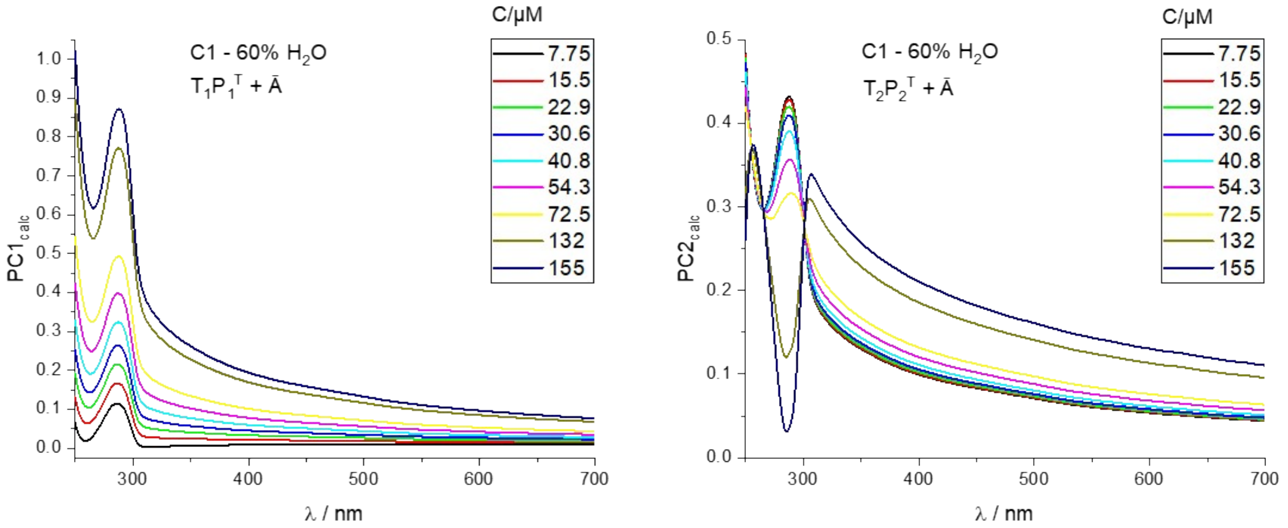

Figure S11: Core data structure for **C1** at 60% H_2O content

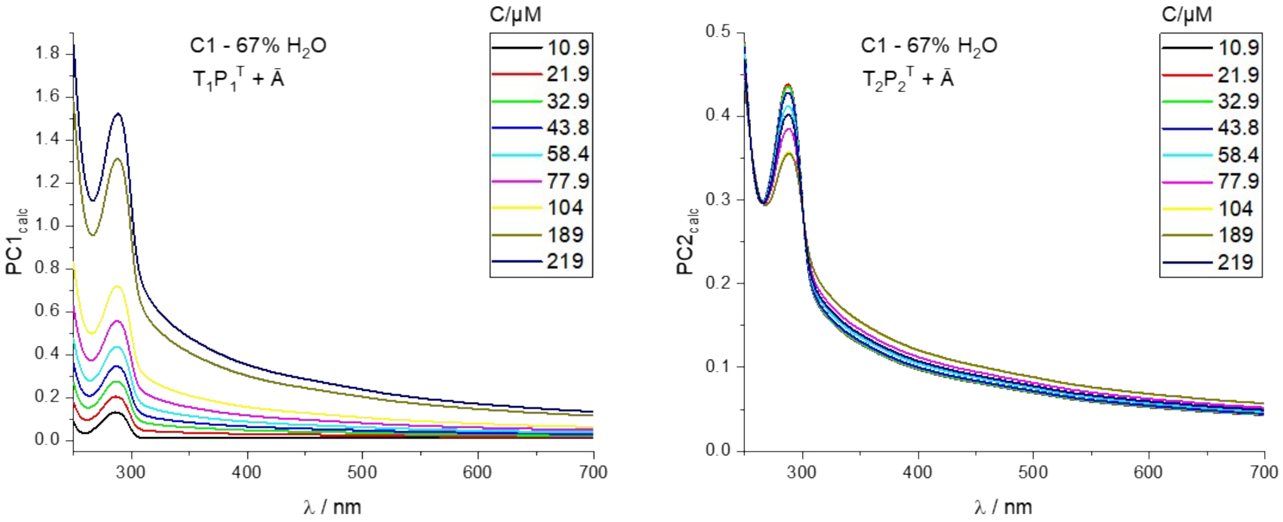

Figure S12: Core data structure for **C1** at 67% H_2O content

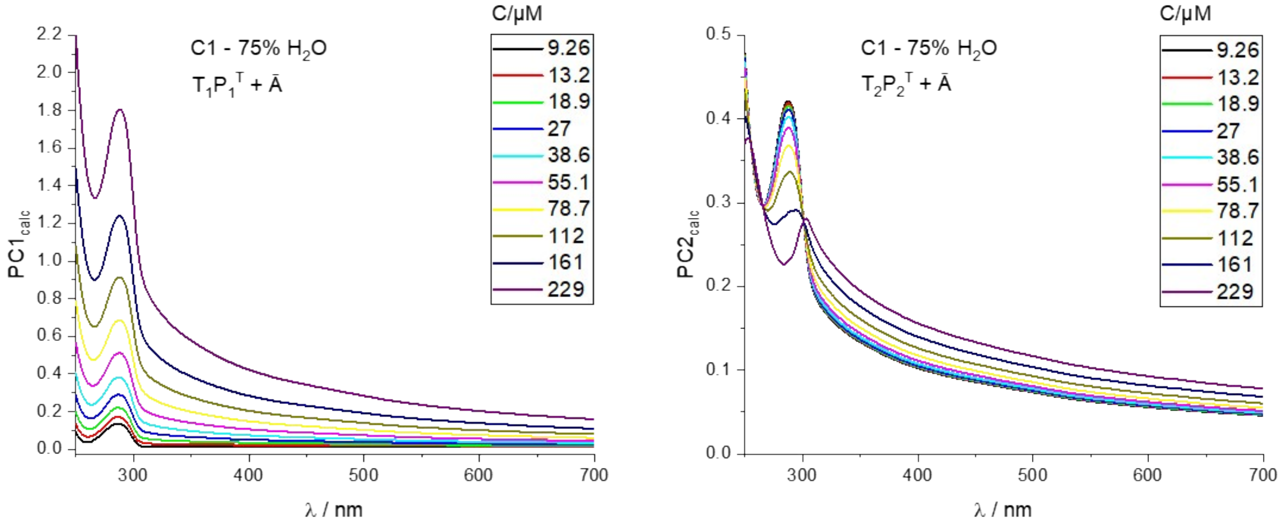

Figure S13: Core data structure for **C1** at 75% H_2O content

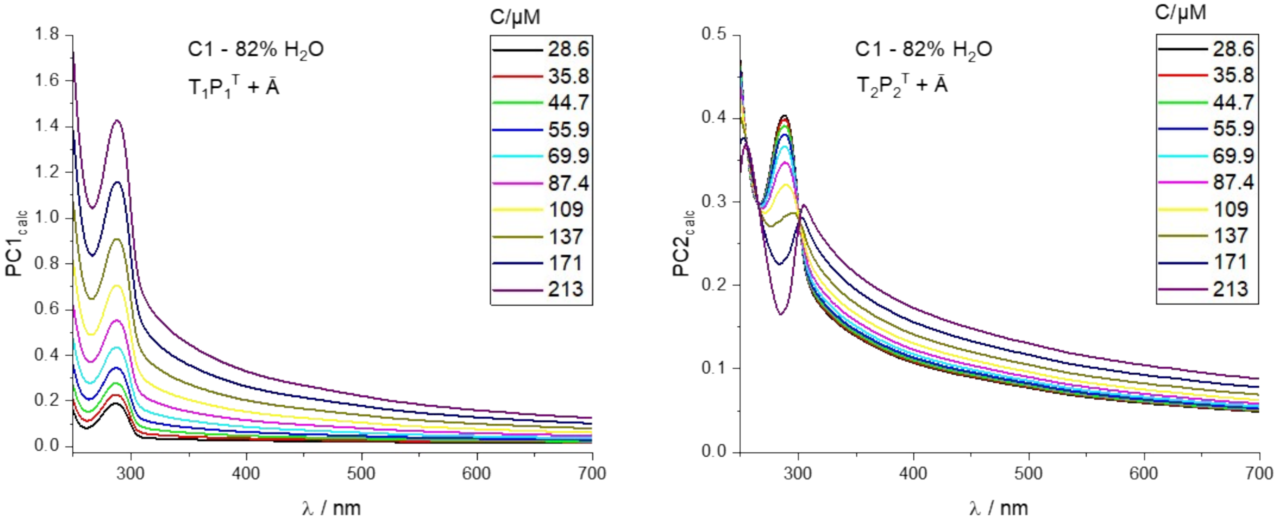

Figure S14: Core data structure for **C1** at 82% H_2O **content**

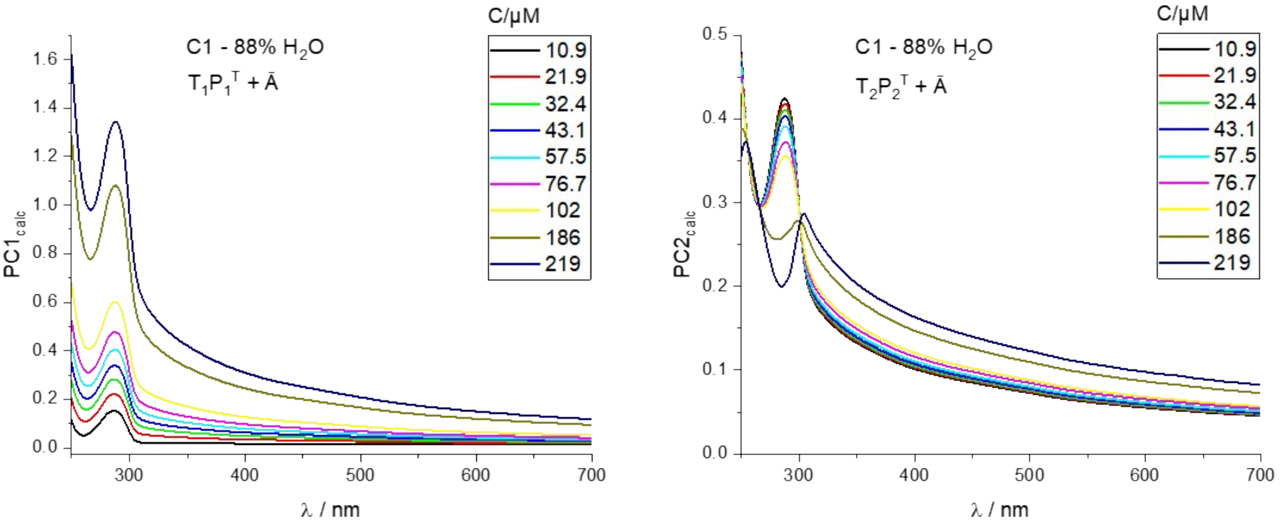

Figure S15: Core data structure for **C1** at 88% H_2O content

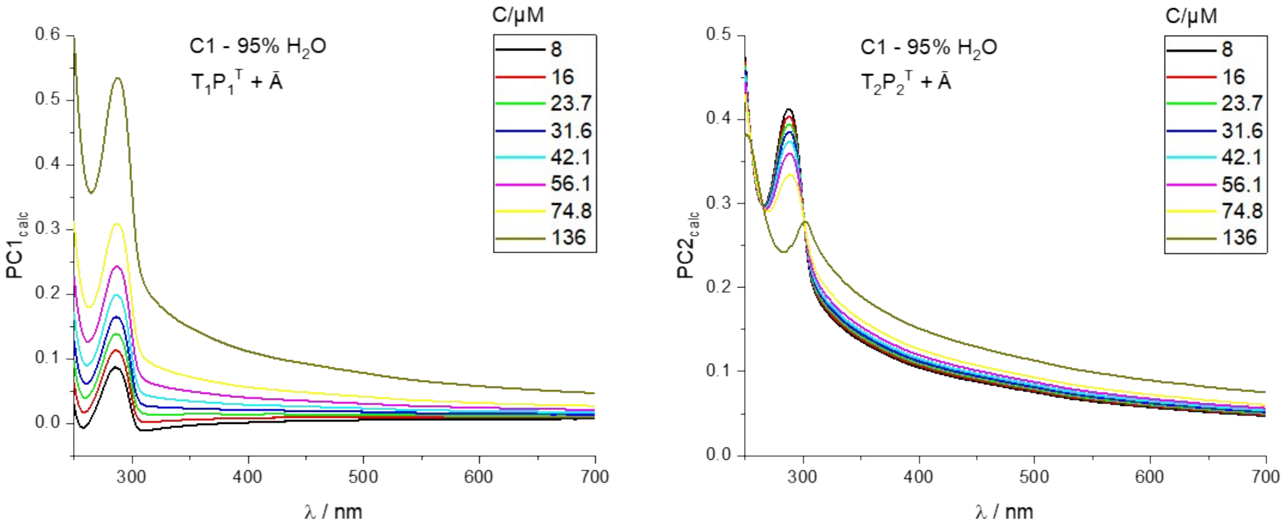

Figure S16: Core data structure for **C1** at 95% H_2O content

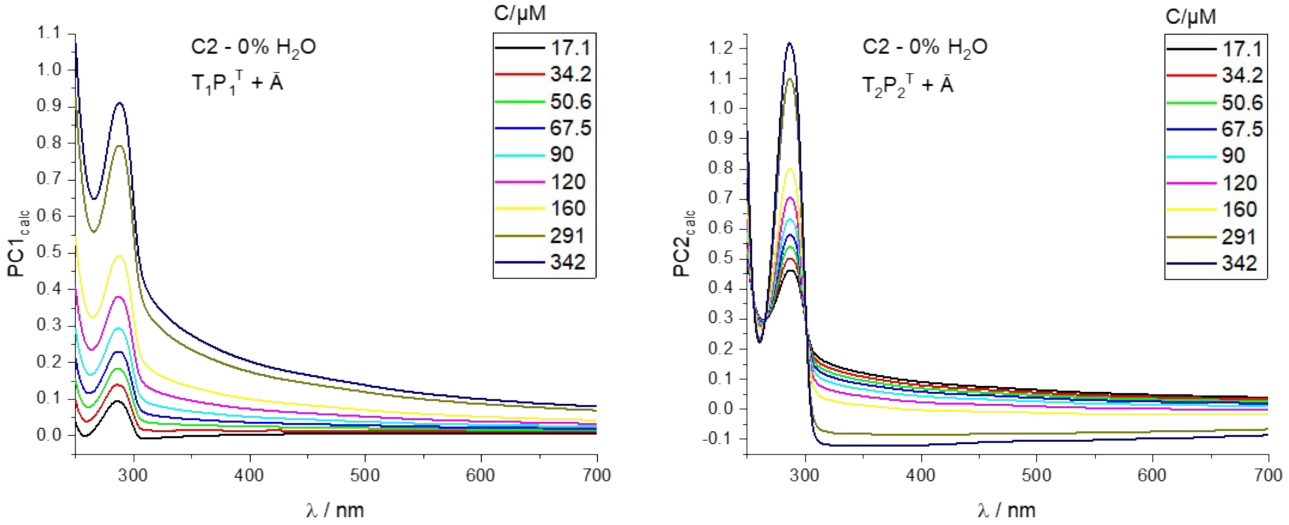

Figure S17: Core data structure for **C2** at 0% H_2O content

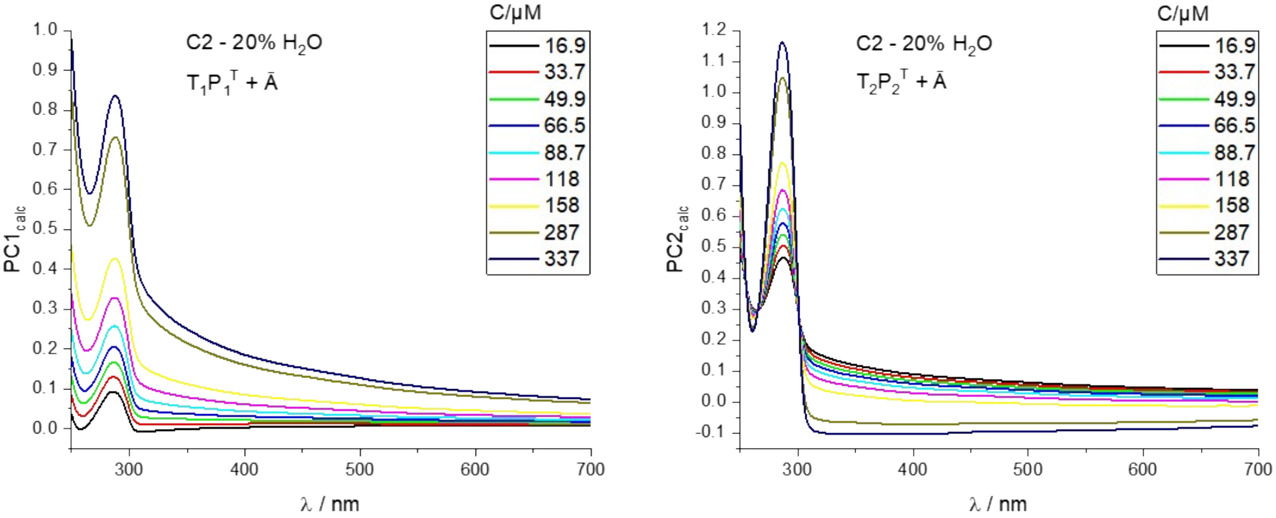

Figure S18: Core data structure for **C2** at 20% H_2O content

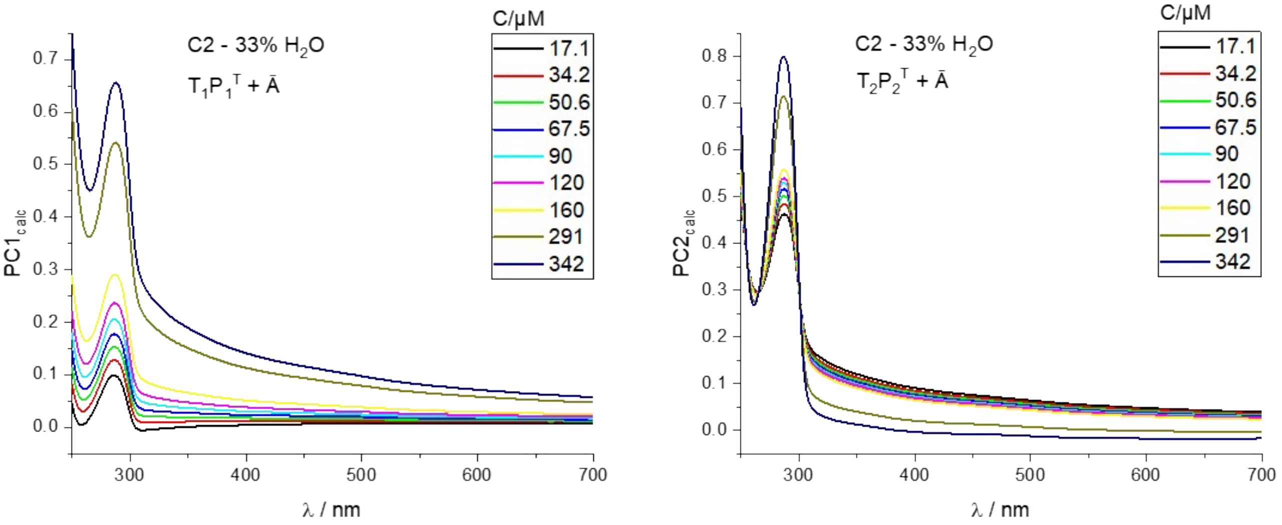

Figure S19: Core data structure for **C2** at 33% H_2O content

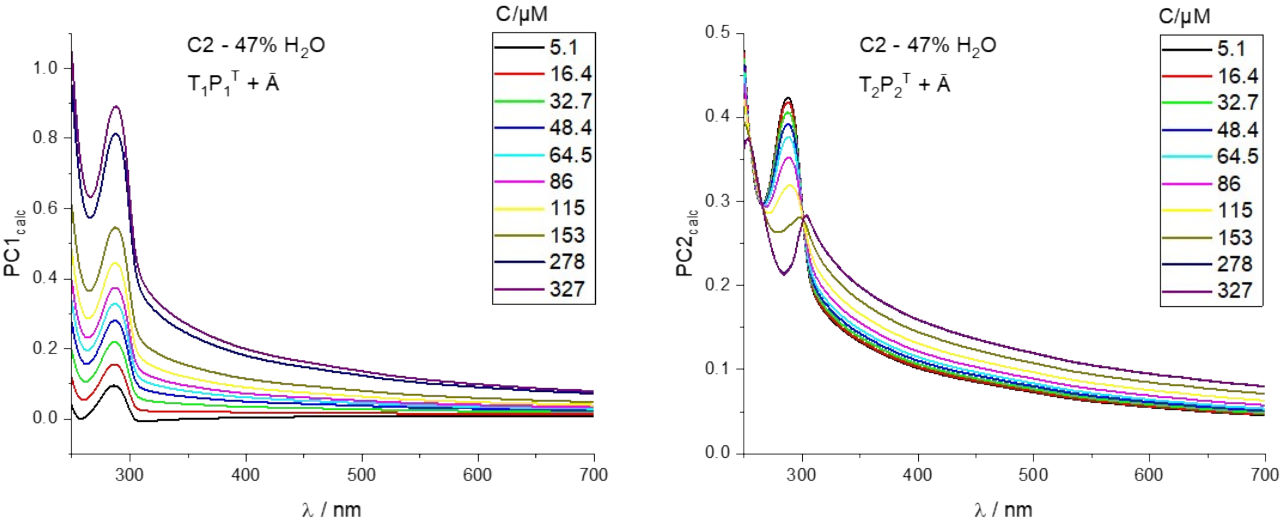

Figure S20: Core data structure for **C2** at 47% H_2O content

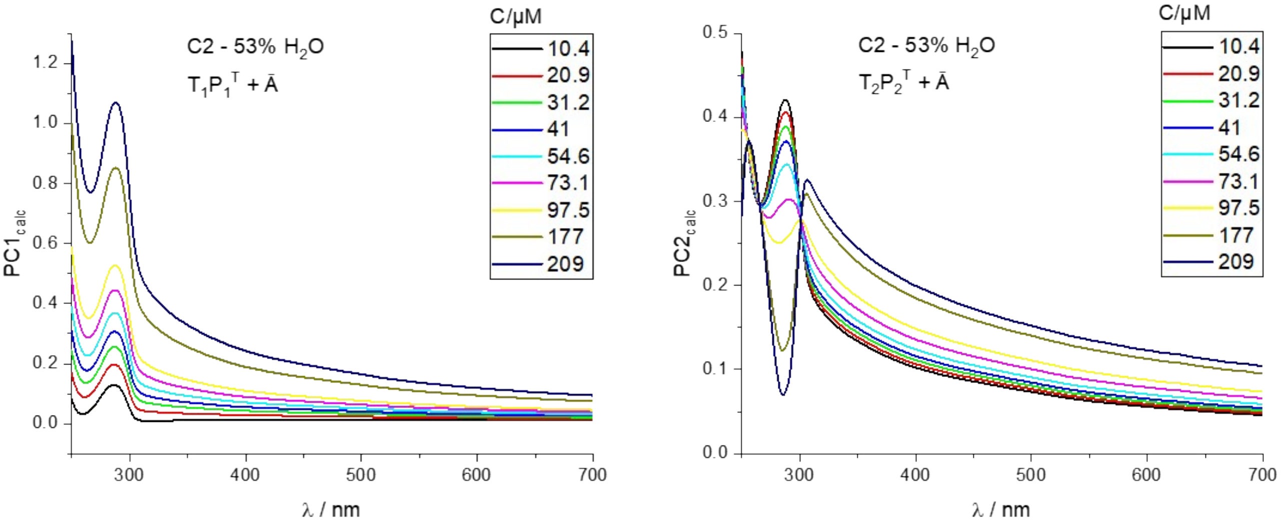

Figure S21: Core data structure for **C2** at 53% H_2O content

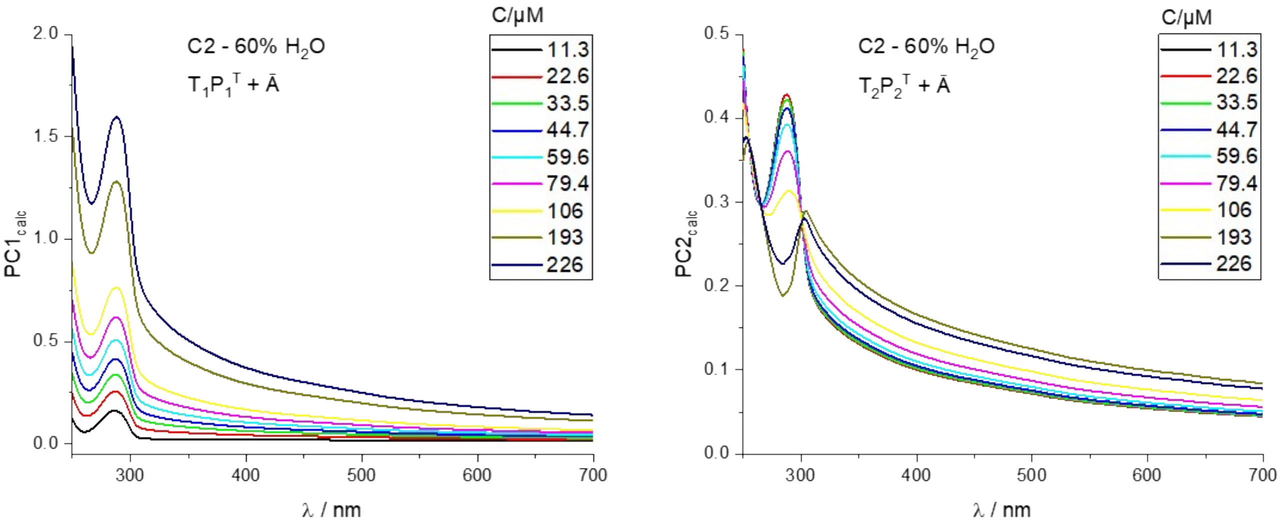

Figure S22: Core data structure for **C2** at 60% H_2O content

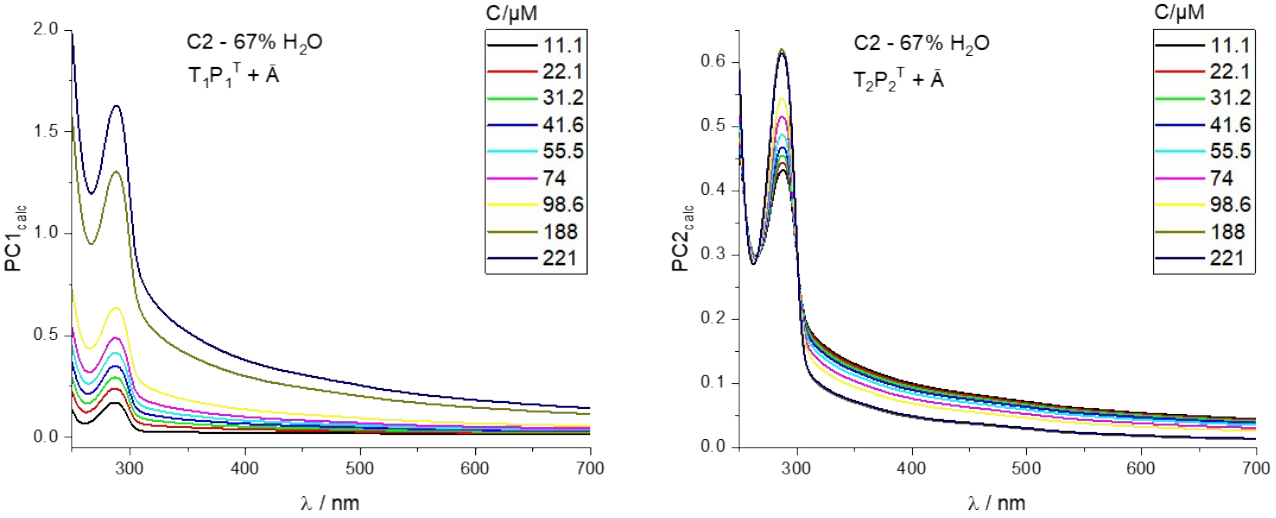

Figure S23: Core data structure for **C2** at 67% H_2O content

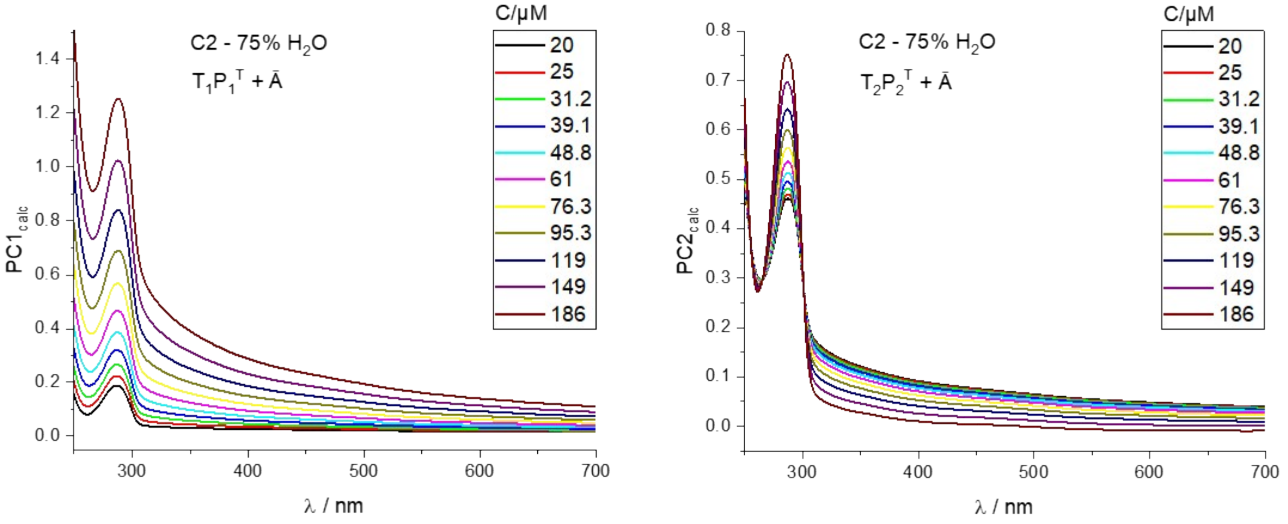

Figure S24: Core data structure for **C2** at 75% H_2O content

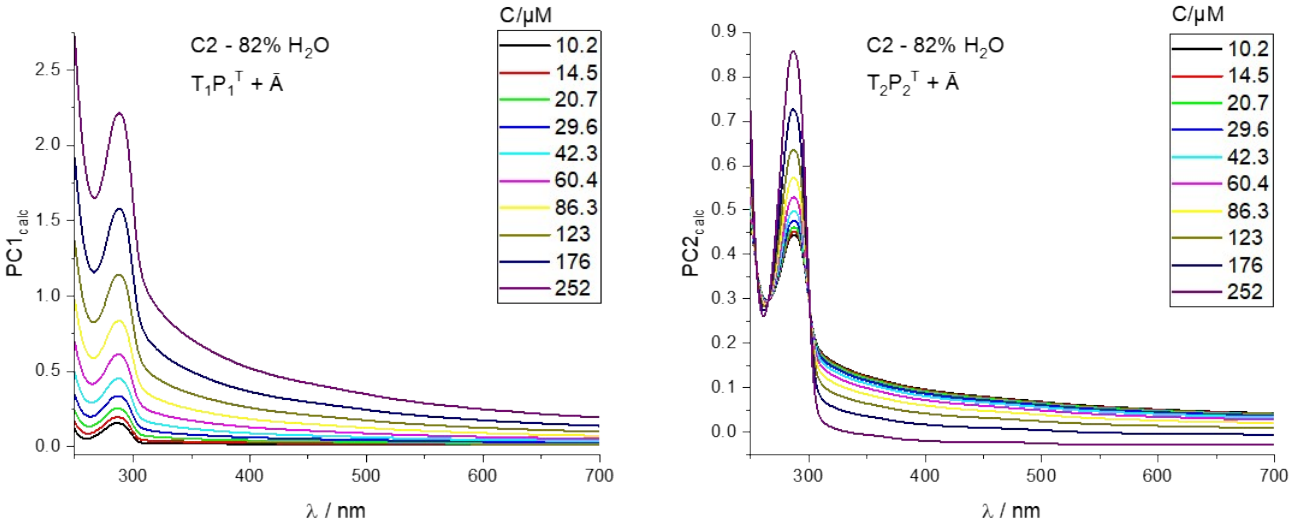

Figure S25: Core data structure for **C2** at 82% H_2O content

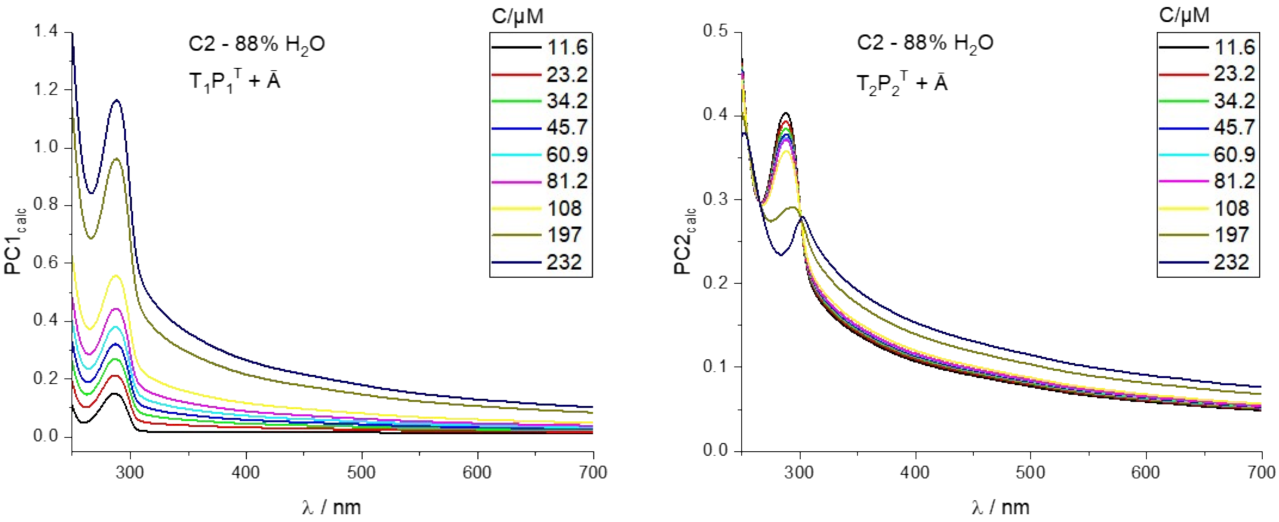

Figure S26: Core data structure for **C2** at 88% H_2O content

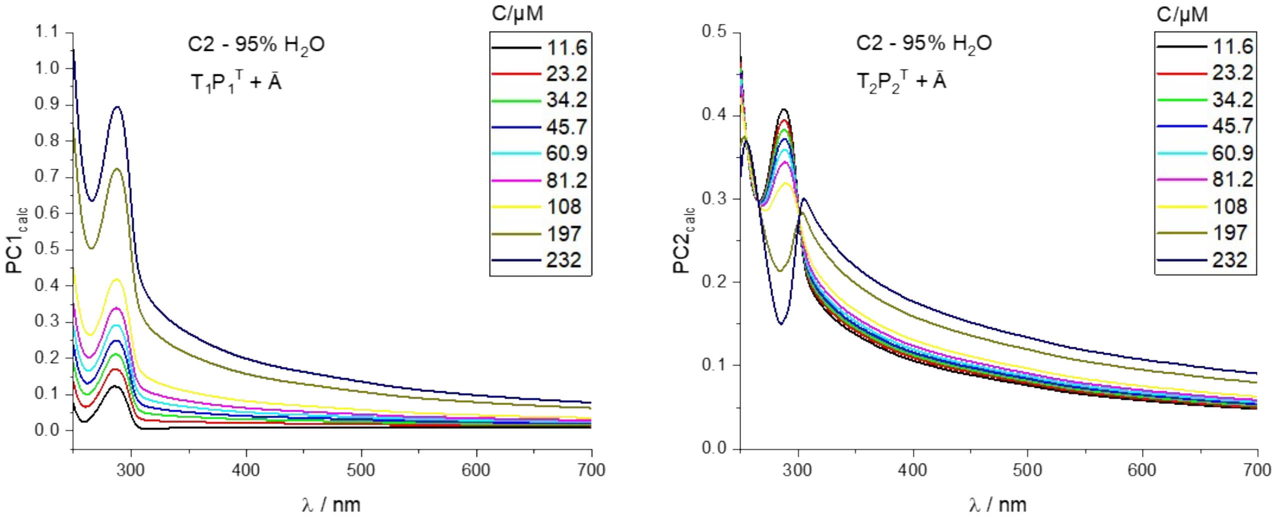

Figure S27: Core data structure for **C2** at 95% H_2O content

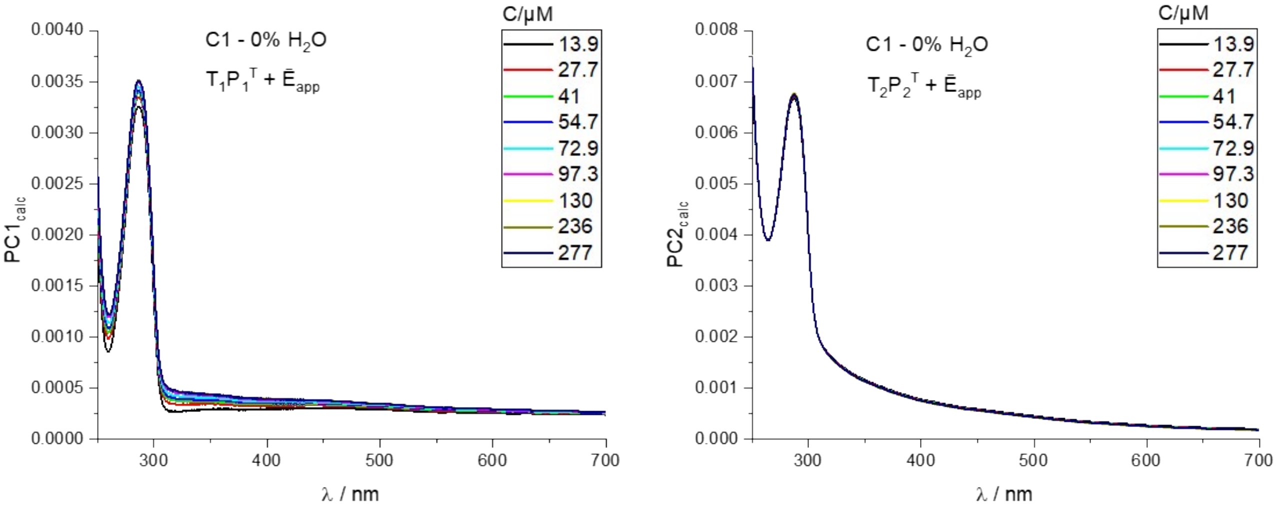

Figure S28: Normalized core data structure for **C1** at 0% H_2O content

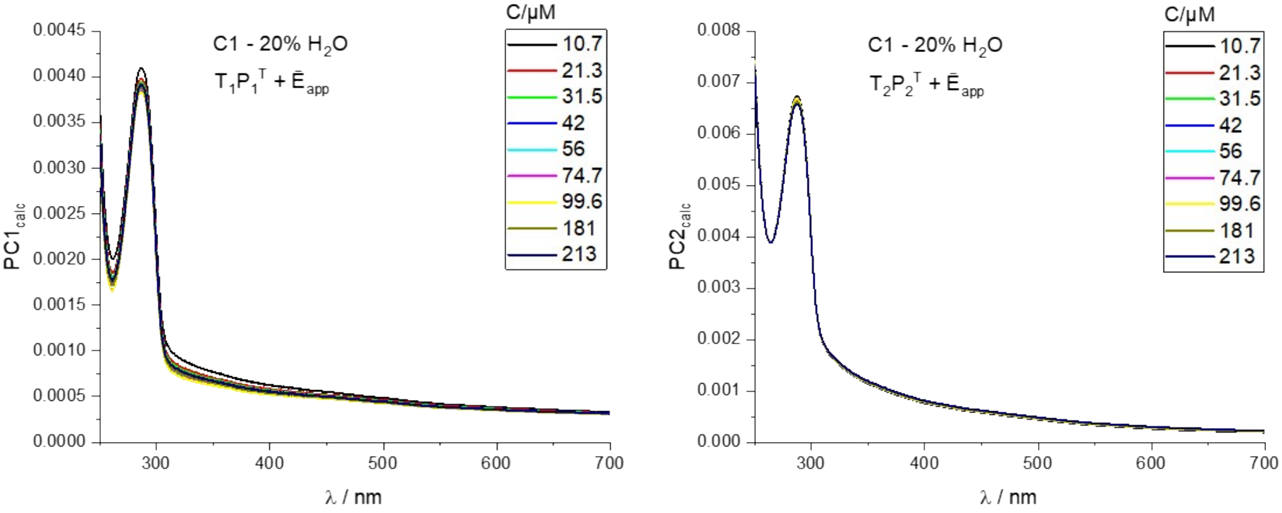

Figure S29: Normalized core data structure for **C1** at 20% H_2O content

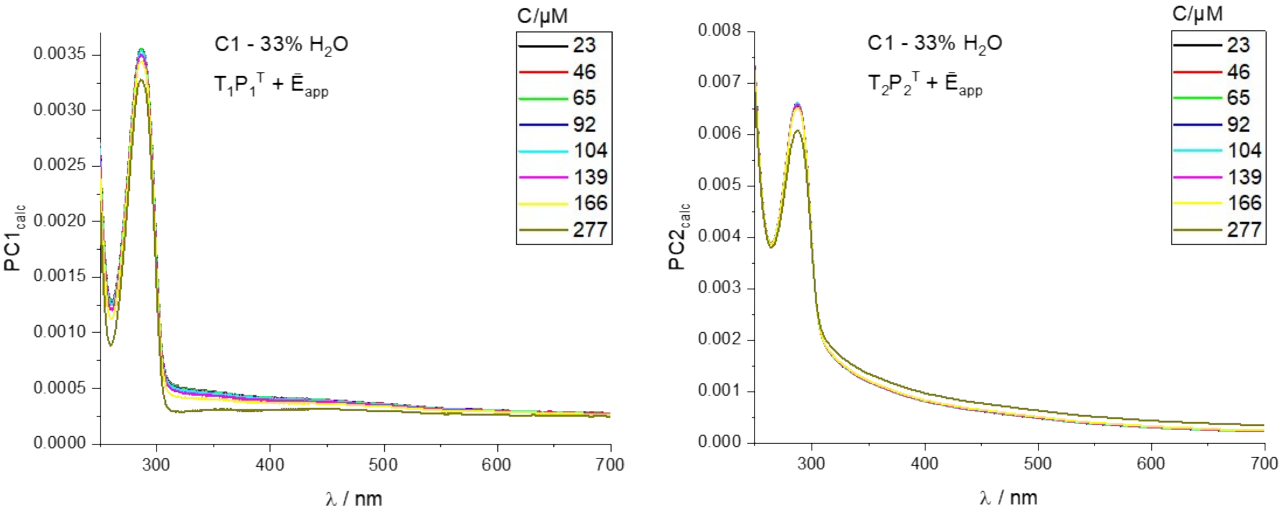

Figure S30: Normalized core data structure for **C1** at 33% H_2O content

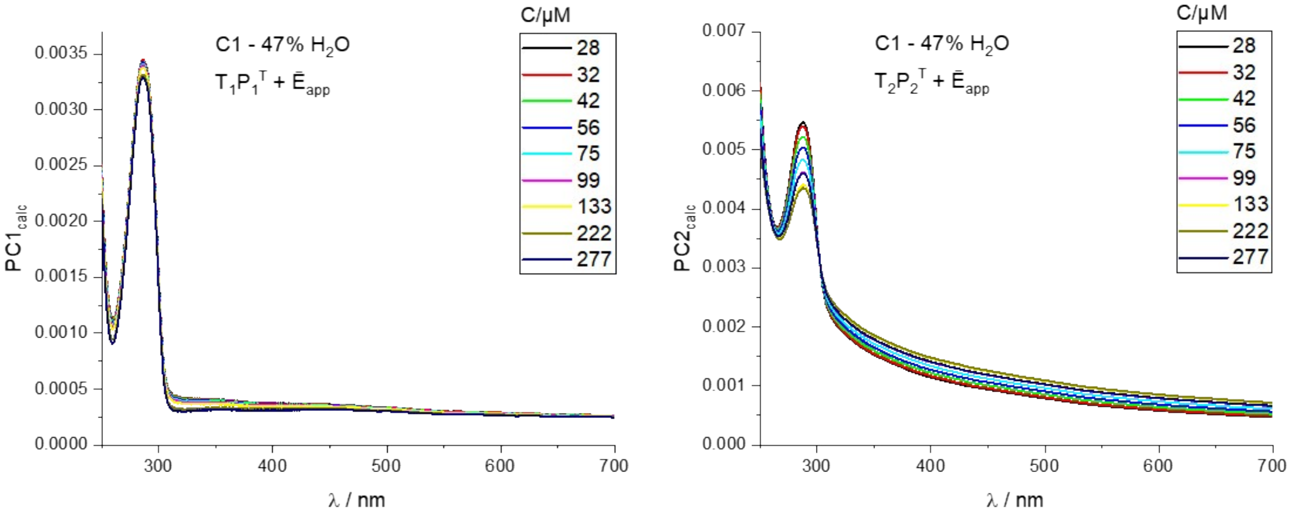

Figure S31: Normalized core data structure for **C1** at 47% H_2O content

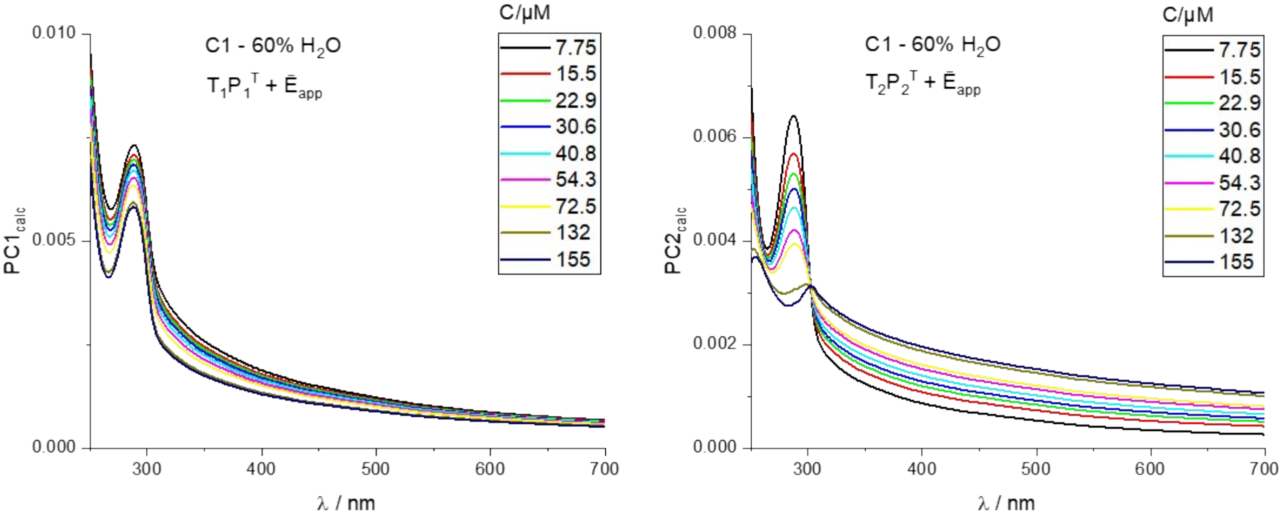

Figure S33: Normalized core data structure for **C1** at 60% H_2O content

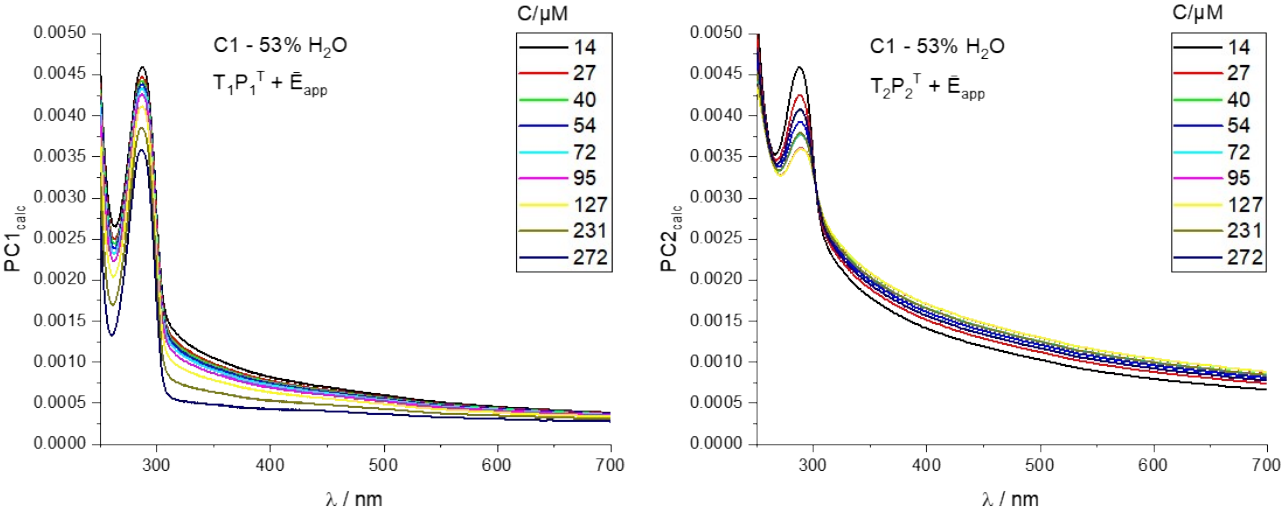

Figure S32: Normalized core data structure for **C1** at 53% H_2O content

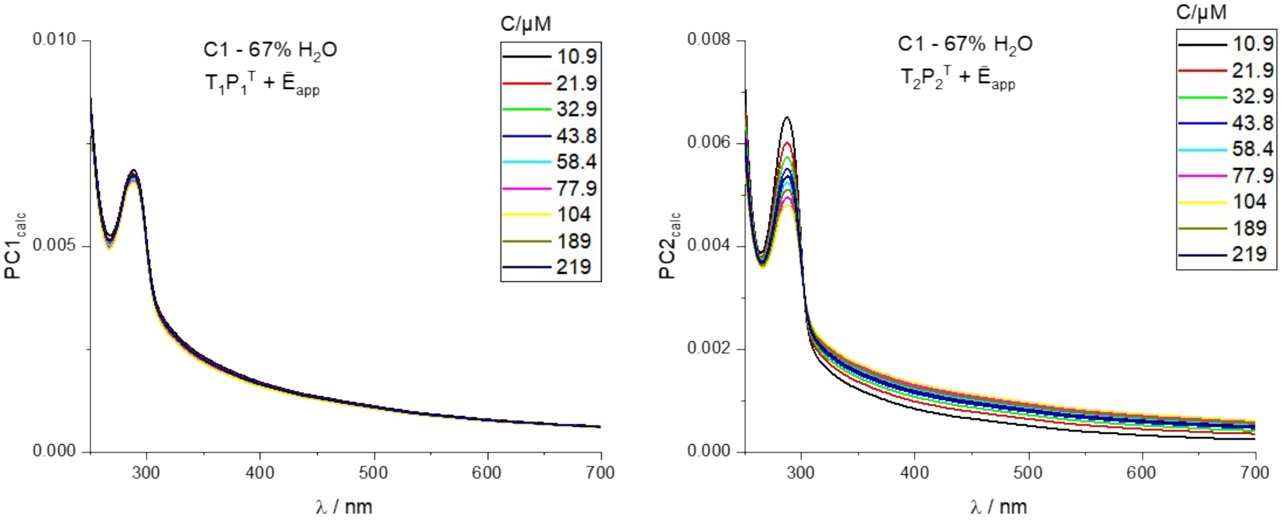

Figure S34: Normalized core data structure for **C1** at 67% H_2O content

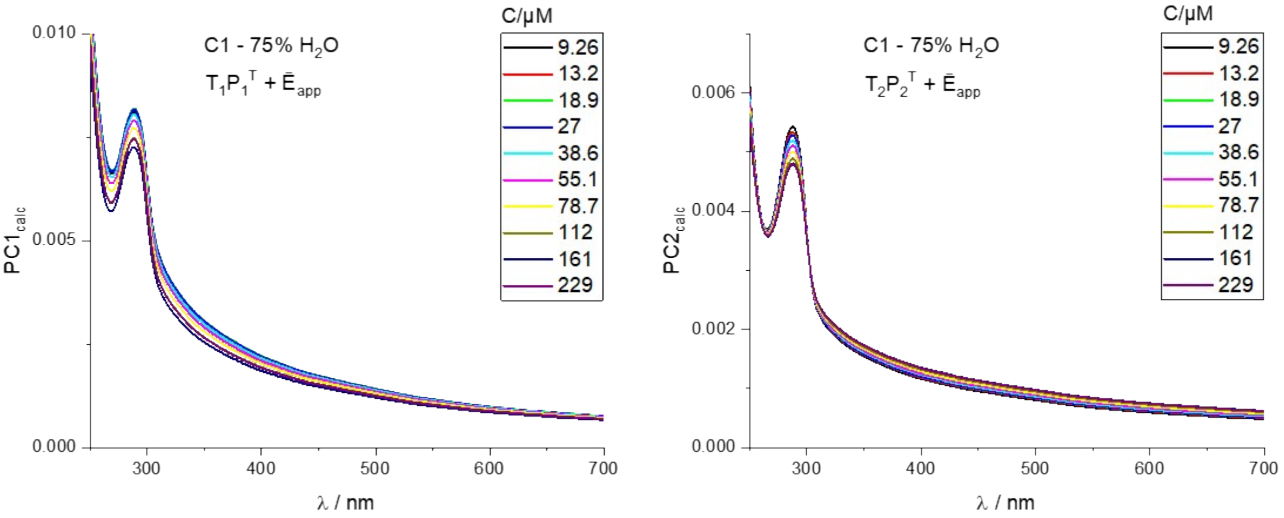

Figure S35: Normalized core data structure for **C1** at 75% H_2O content

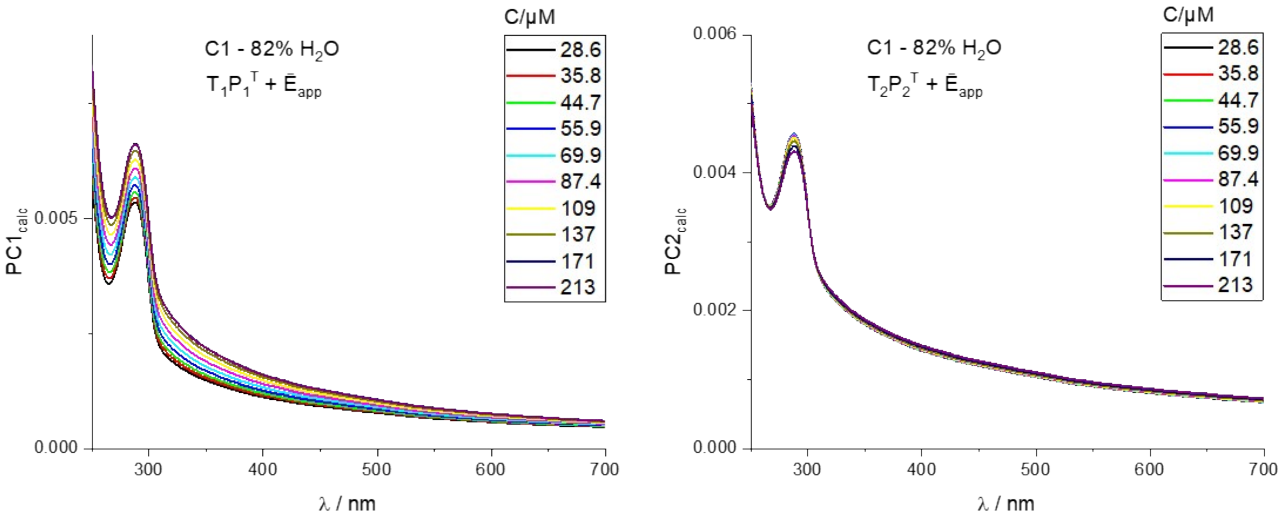

Figure S36: Normalized core data structure for **C1** at 82% H_2O content

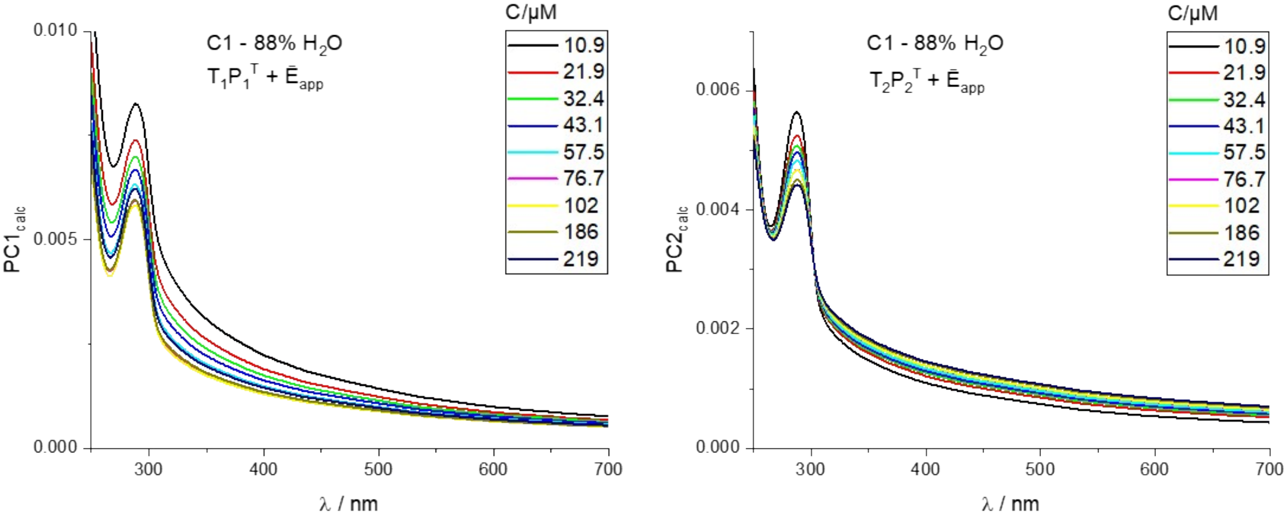

Figure S37: Normalized core data structure for **C1** at 88% H_2O content

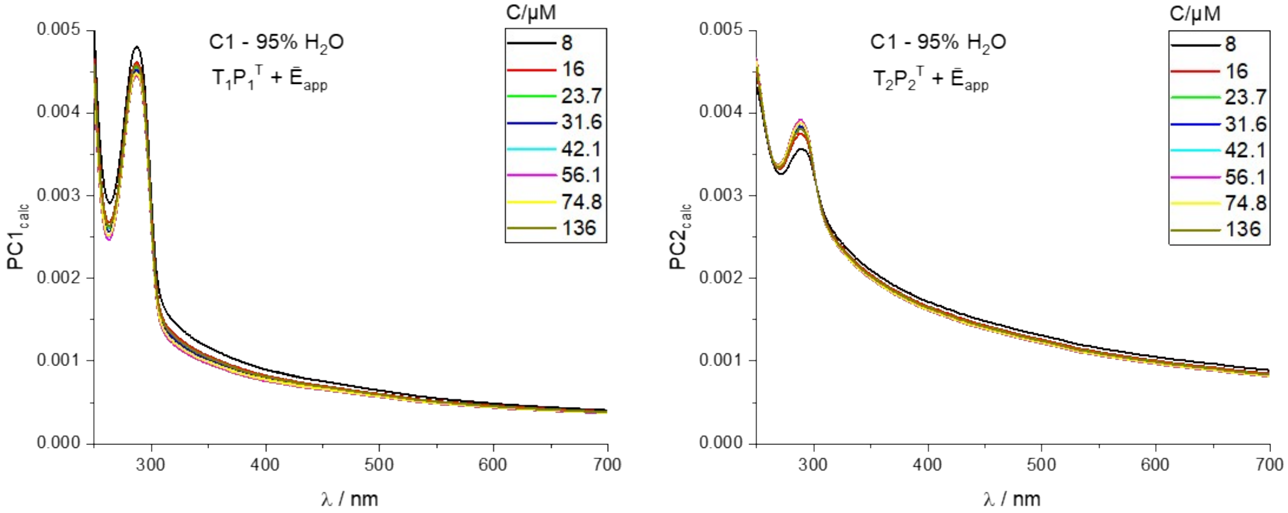

Figure S38: Normalized core data structure for **C1** at 95% H_2O content

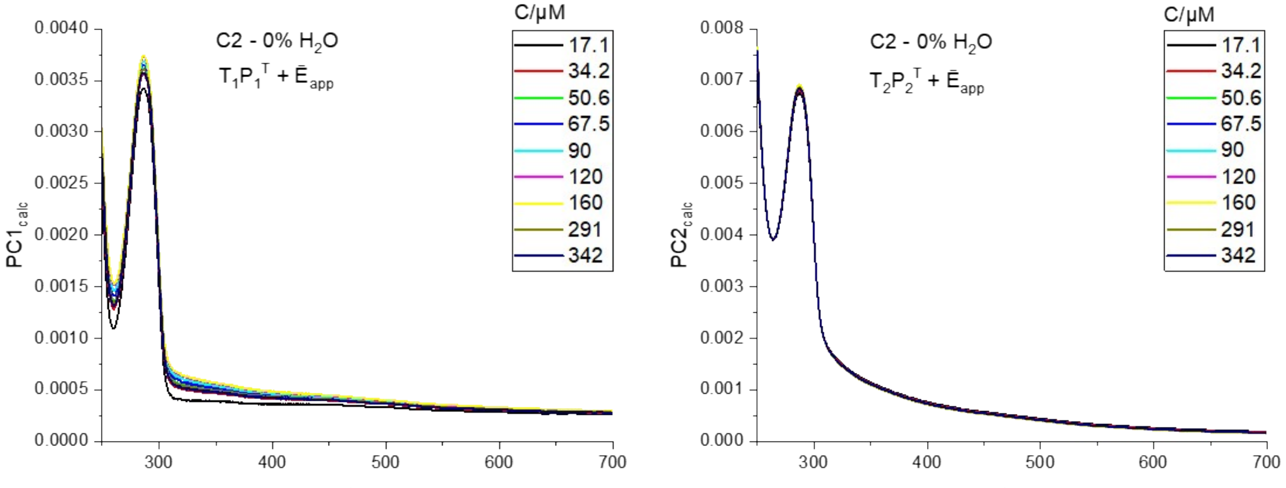

Figure S39: Normalized core data structure for **C2** at 0% H_2O content

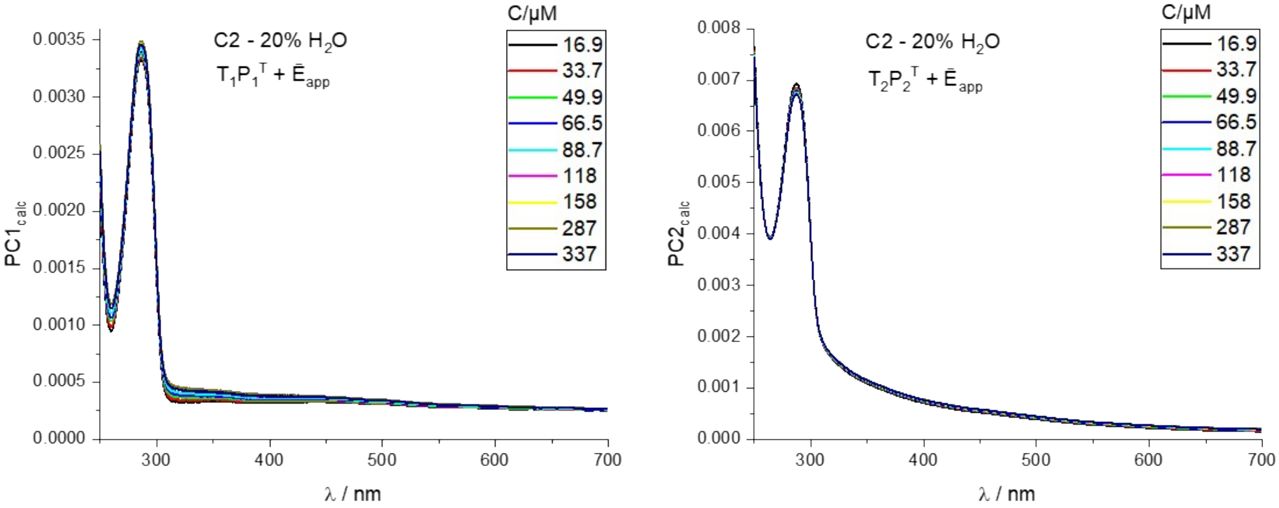

Figure S40: Normalized core data structure for **C2** at 20% H_2O content

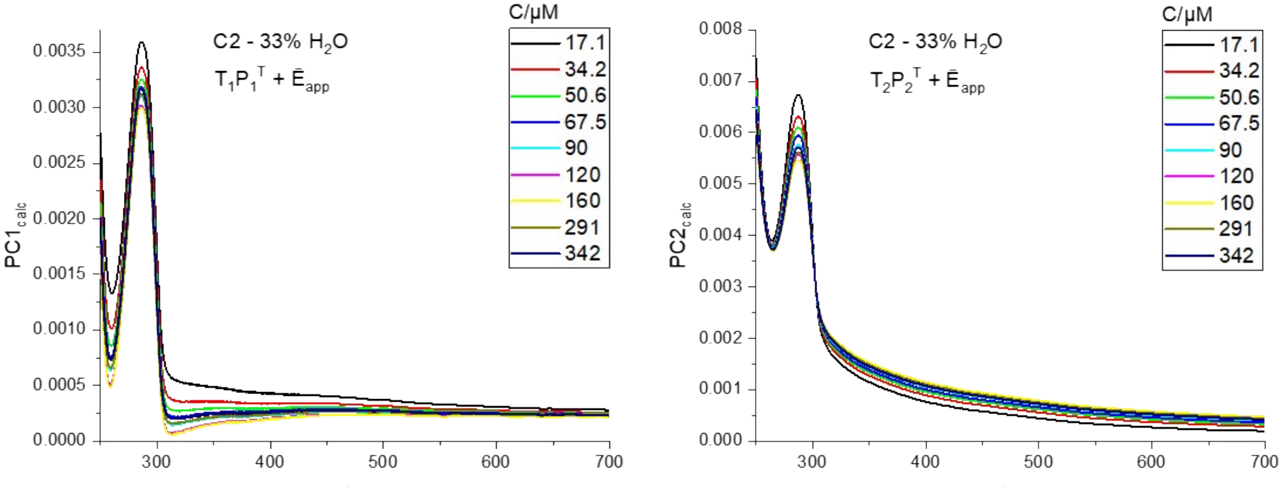

Figure S41: Normalized core data structure for **C2** at 33% H_2O content

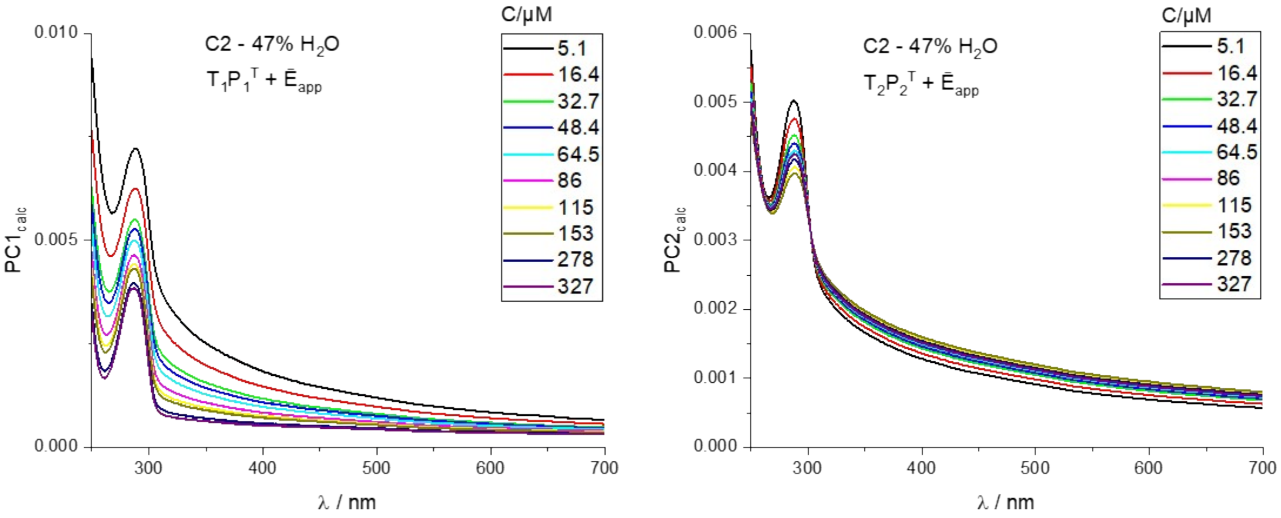

Figure S42: Normalized core data structure for **C2** at 47% H_2O content

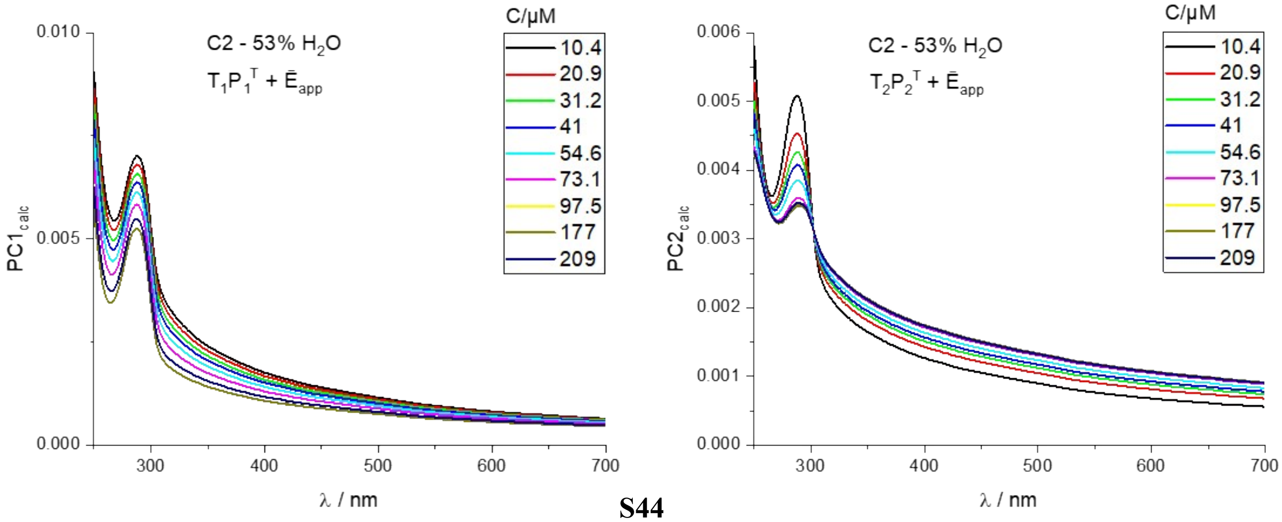

Figure S43: Normalized core data structure for **C2** at 53% H_2O content

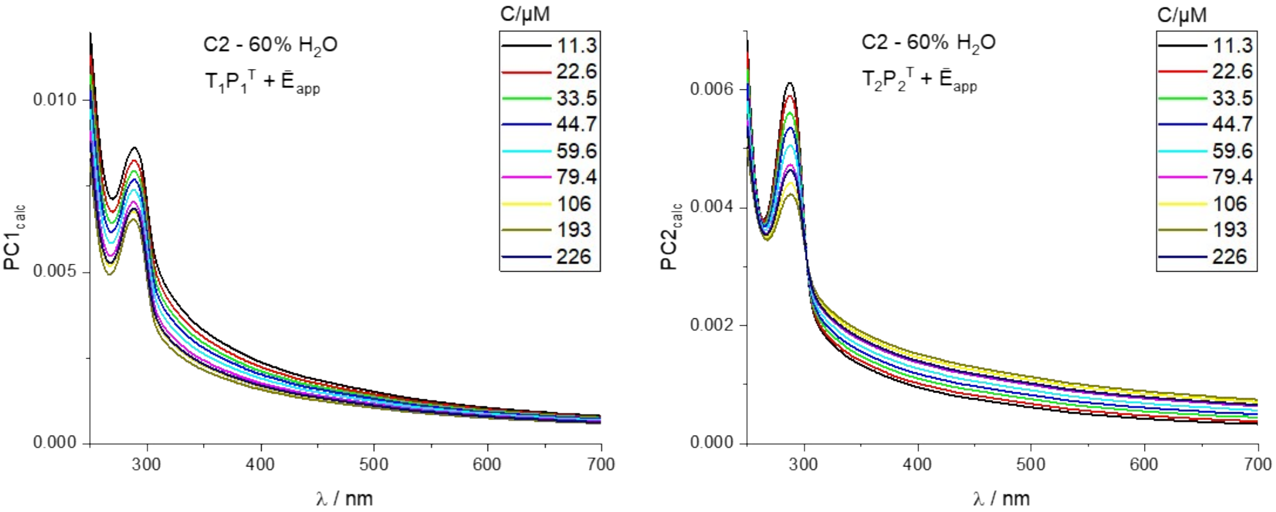

Figure S44: Normalized core data structure for **C2** at 60% H_2O content

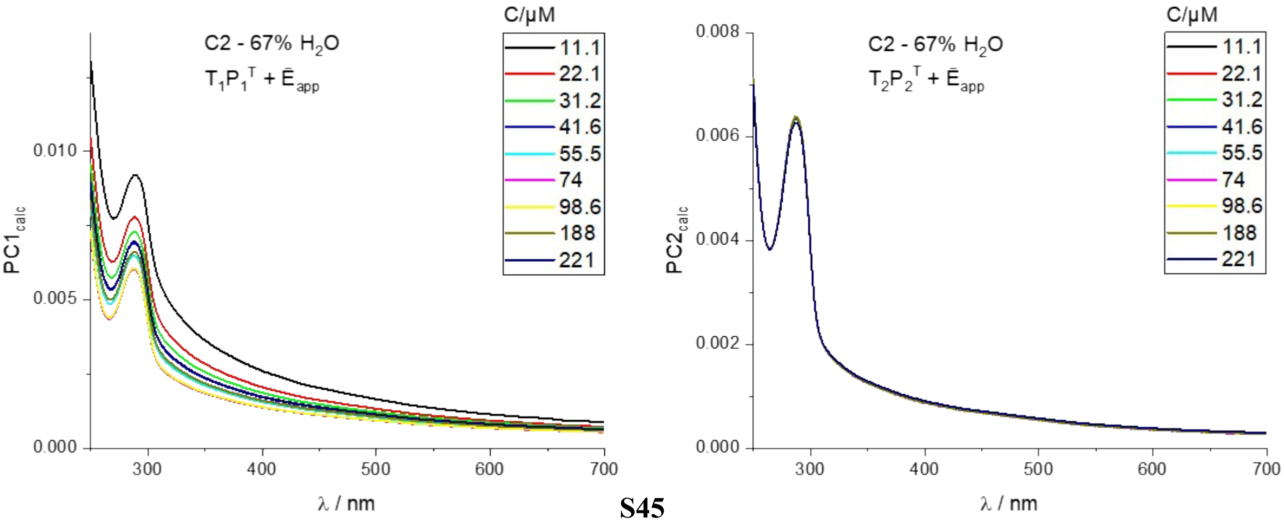

Figure S45: Normalized core data structure for **C2** at 67% H_2O content

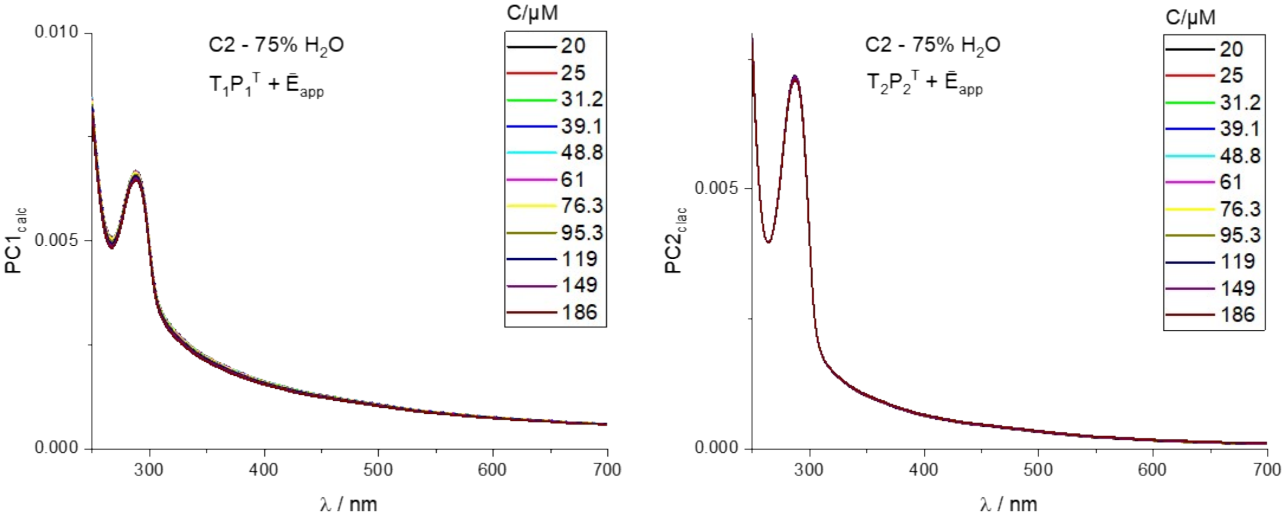

Figure S46: Normalized core data structure for **C2** at 75% H_2O content

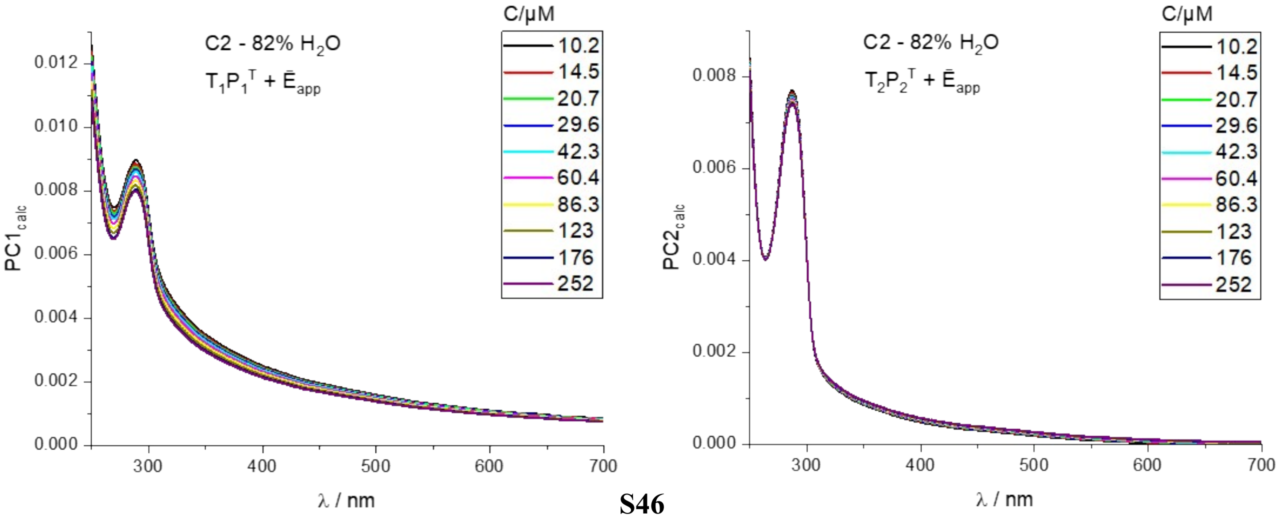

Figure S47: Normalized core data structure for **C2** at 82% H_2O content

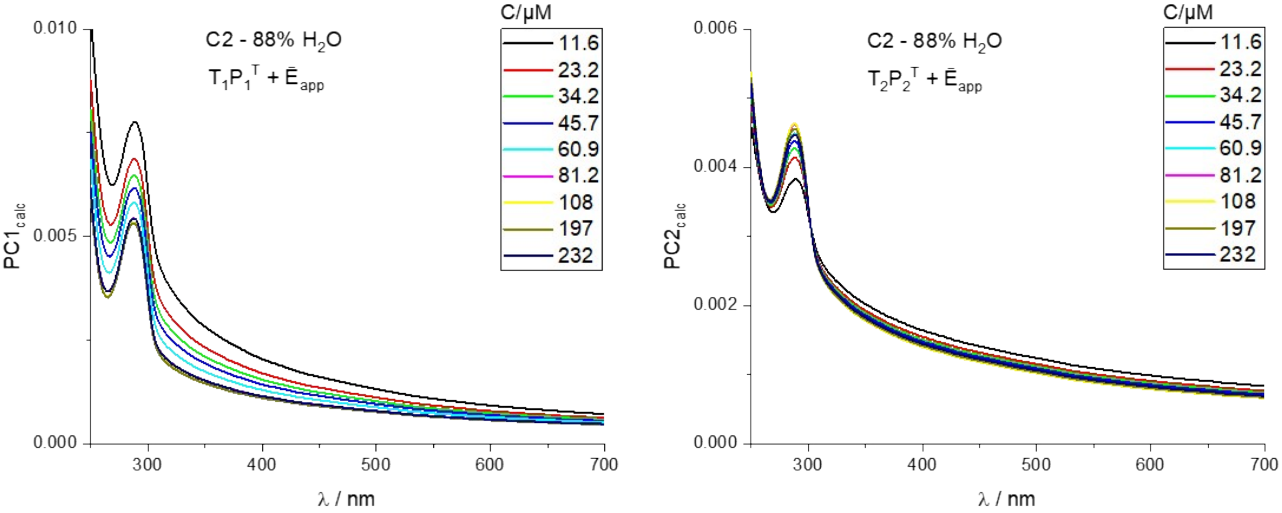

Figure S48: Normalized core data structure for **C2** at 88% H_2O content

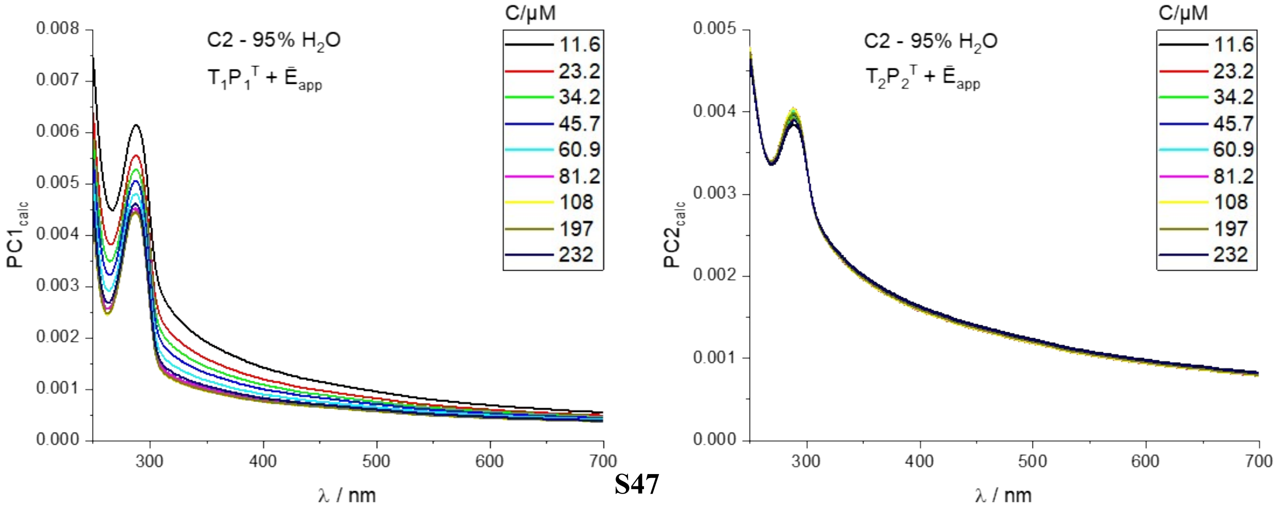

Figure S49: Normalized core data structure for **C2** at 95% H_2O content

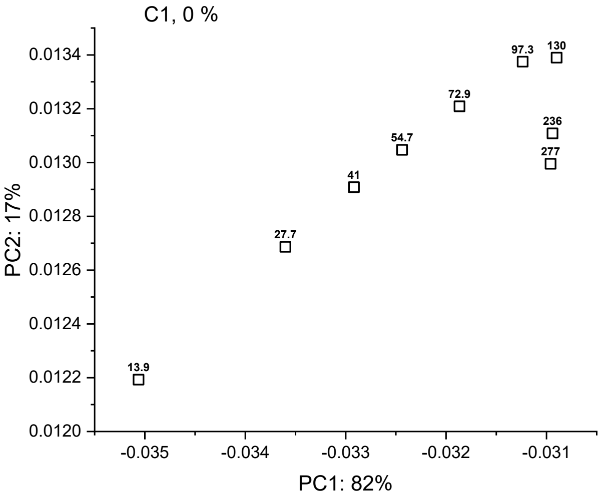

Figure S50: PC2 vs. PC1 scores for **C1** at 0% H_2O content

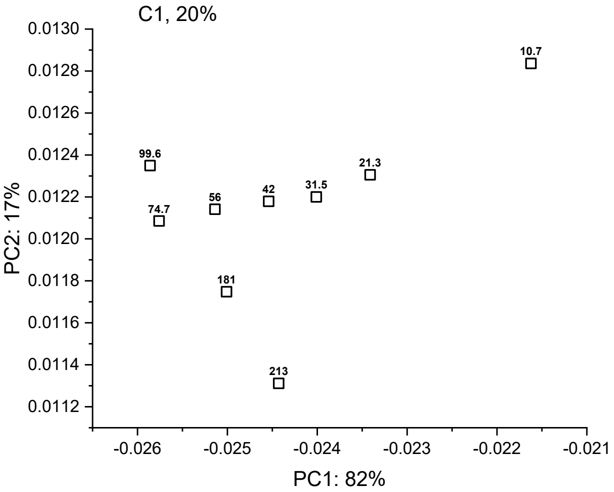

Figure S51: PC2 vs. PC1 scores for **C1** at 20% H_2O content

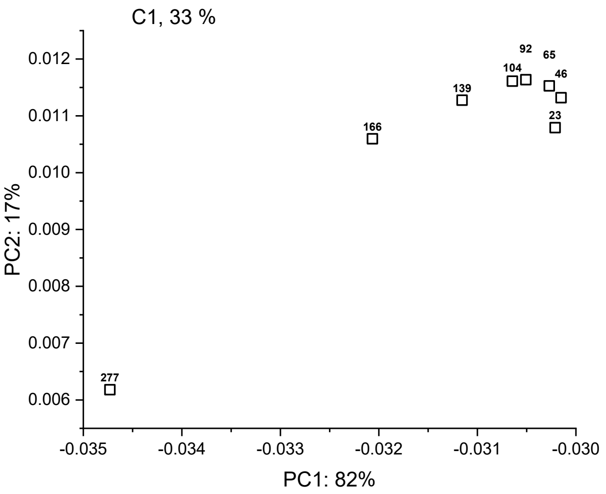

Figure S52: PC2 vs. PC1 scores for **C1** at 33% H_2O content

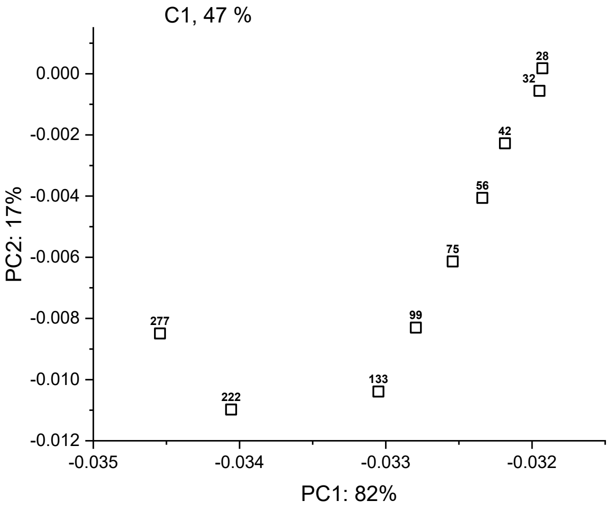

Figure S53: PC2 vs. PC1 scores for **C1** at 47% H_2O content

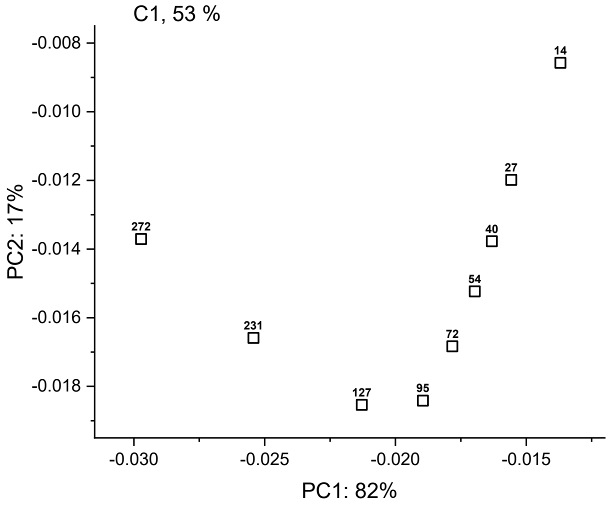

Figure S54: PC2 vs. PC1 scores for **C1** at 53% H_2O content

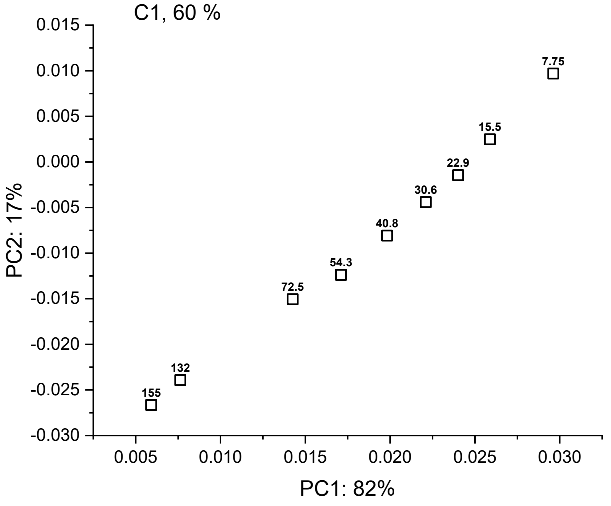

Figure S55: PC2 vs. PC1 scores for **C1** at 60% H_2O content

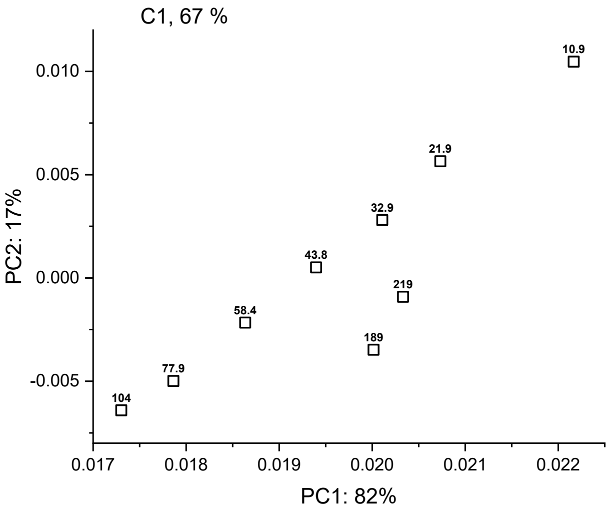

Figure S56: PC2 vs. PC1 scores for **C1** at 67% H_2O content

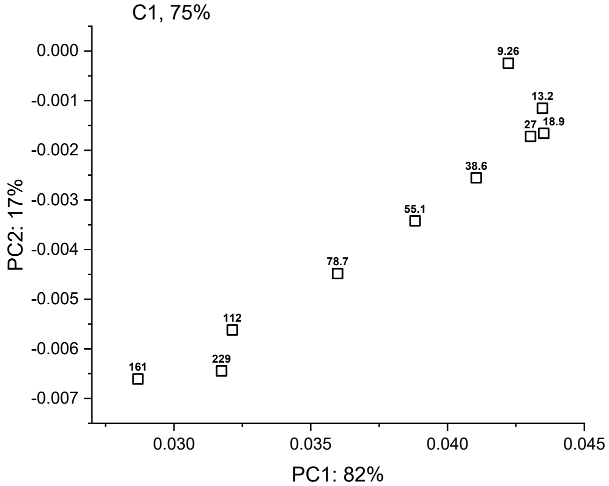

Figure S57: PC2 vs. PC1 scores for **C1** at 75% H_2O content

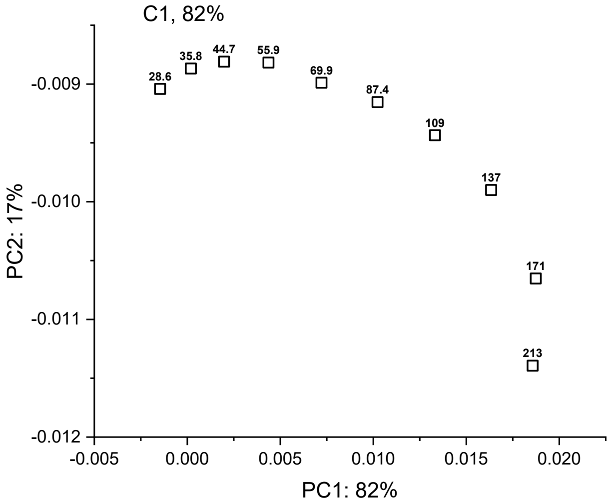

Figure S58: PC2 vs. PC1 scores for **C1** at 82% H_2O content

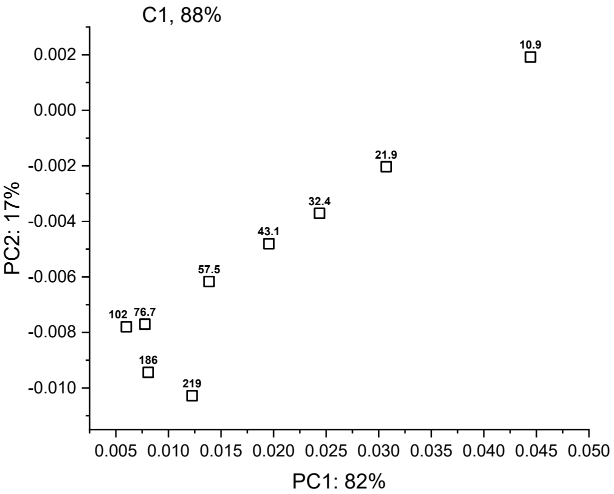

Figure S59: PC2 vs. PC1 scores for **C1** at 88% H_2O content

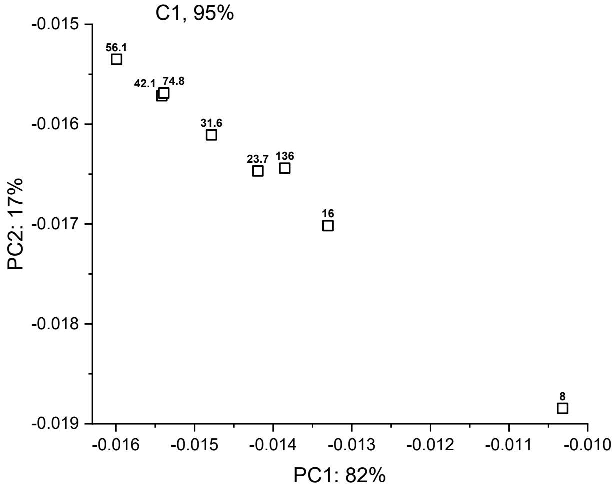

Figure S60: PC2 vs. PC1 scores for **C1** at 95% H_2O content

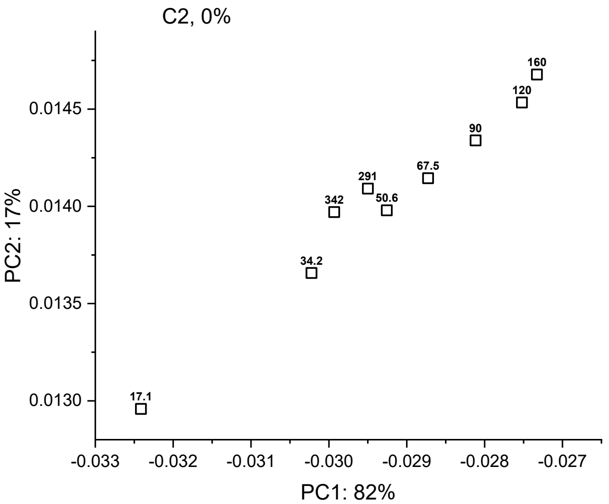

Figure S61: PC2 vs. PC1 scores for **C2** at 0% H_2O content

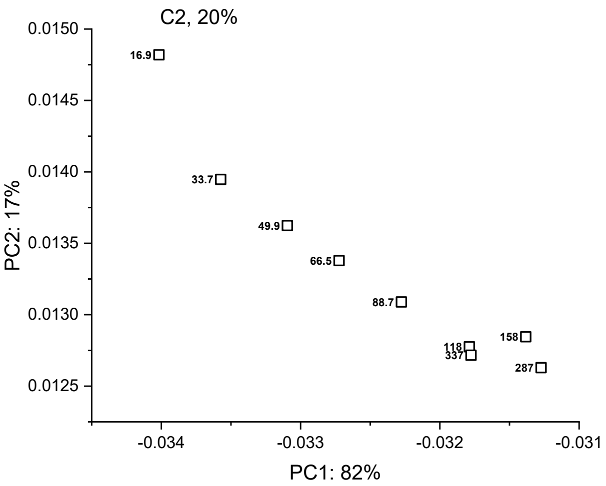

Figure S62: PC2 vs. PC1 scores for **C2** at 20% H_2O content

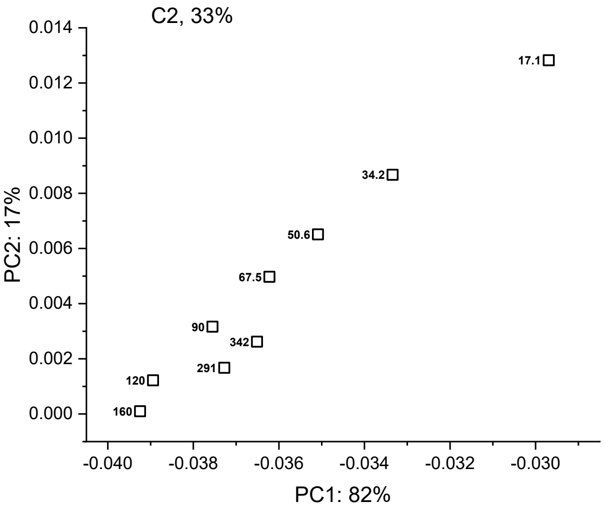

Figure S63: PC2 vs. PC1 scores for **C2** at 33% H_2O content

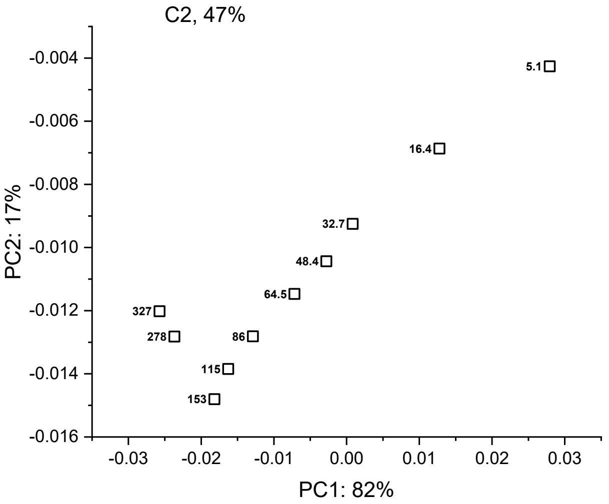

Figure S64: PC2 vs. PC1 scores for **C2** at 47% H_2O content

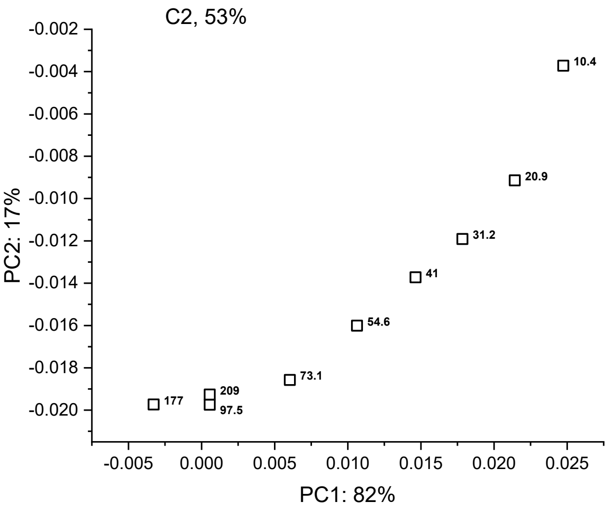

Figure S65: PC2 vs. PC1 scores for **C2** at 53% H_2O content

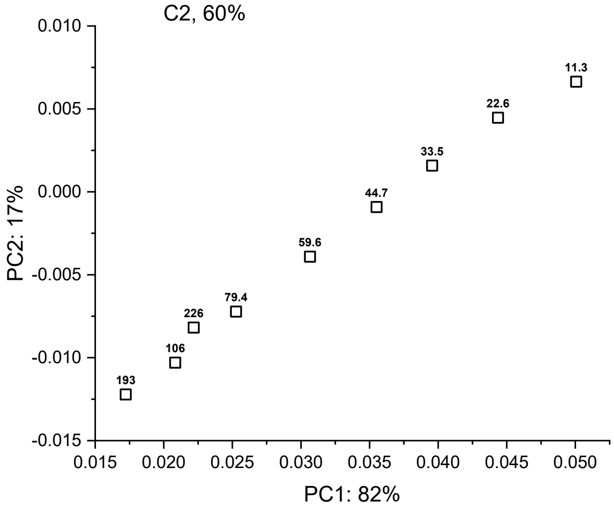

Figure S66: PC2 vs. PC1 scores for **C2** at 60% H_2O content

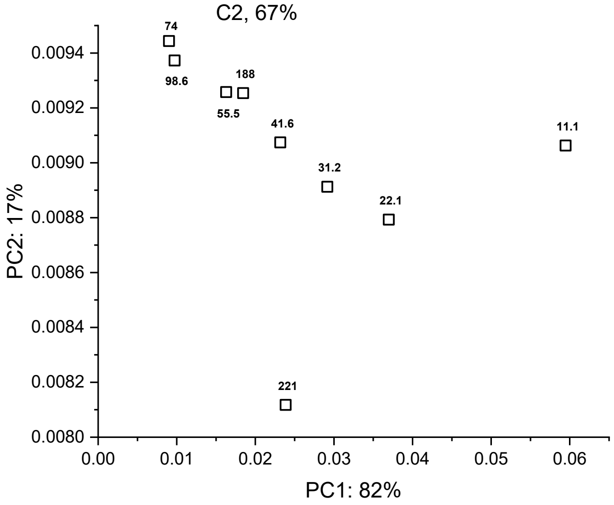

Figure S67: PC2 vs. PC1 scores for **C2** at 67% H_2O content

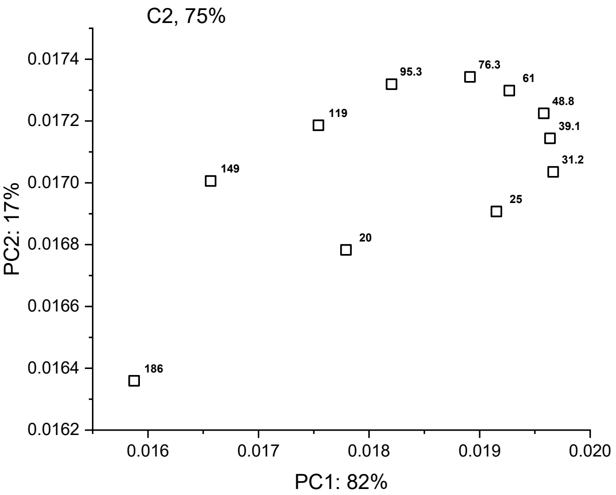

Figure S68: PC2 vs. PC1 scores for **C2** at 75% H_2O content

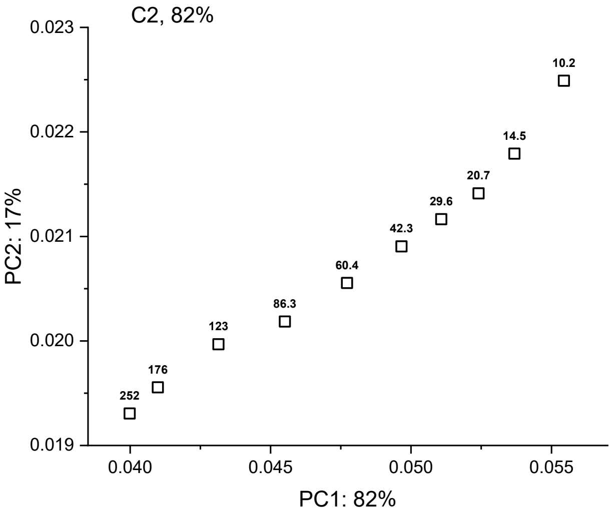

Figure S69: PC2 vs. PC1 scores for **C2** at 82% H_2O content

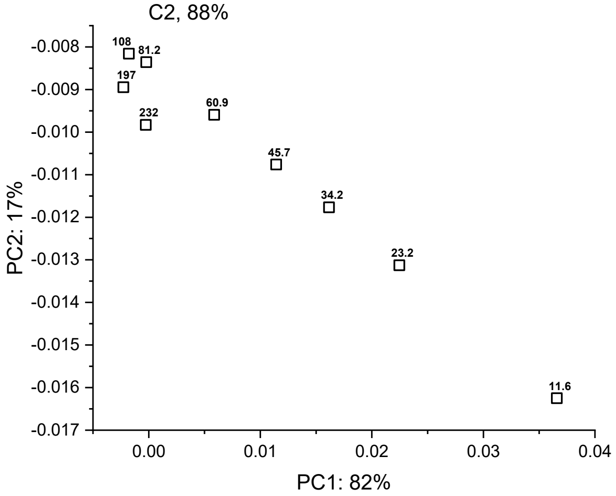

Figure S70: PC2 vs. PC1 scores for **C2** at 88% H_2O content

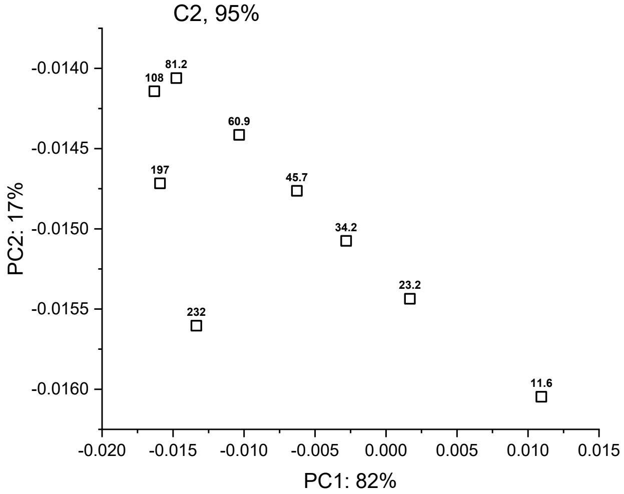

Figure S71: PC2 vs. PC1 scores for **C2** at 95% H_2O content

Table S1. DLS measurement of **C1** in THF (67%) / H_2O (33%)

Measurement ID	Measurement name	PdI	Maximum of the distribution in Intensity (nm)		
			Peak 1	Peak 2	Peak 3
1	C133 1	-	3.699	620.6	5125
2	C133 2	-	3.496	410.2	5516
3	C133 3	-	3.504	601.7	4989
4	C133 4	-	3.491	569.5	5189
5	C133 5	-	3.468	530.2	5033
6	C133 6	-	3.425	486.7	5370
Average ±SD (%)		-	3.51 ± 0.09 (81.4)	536 ± 79 (11.9)	5204 ± 203 (3.9)

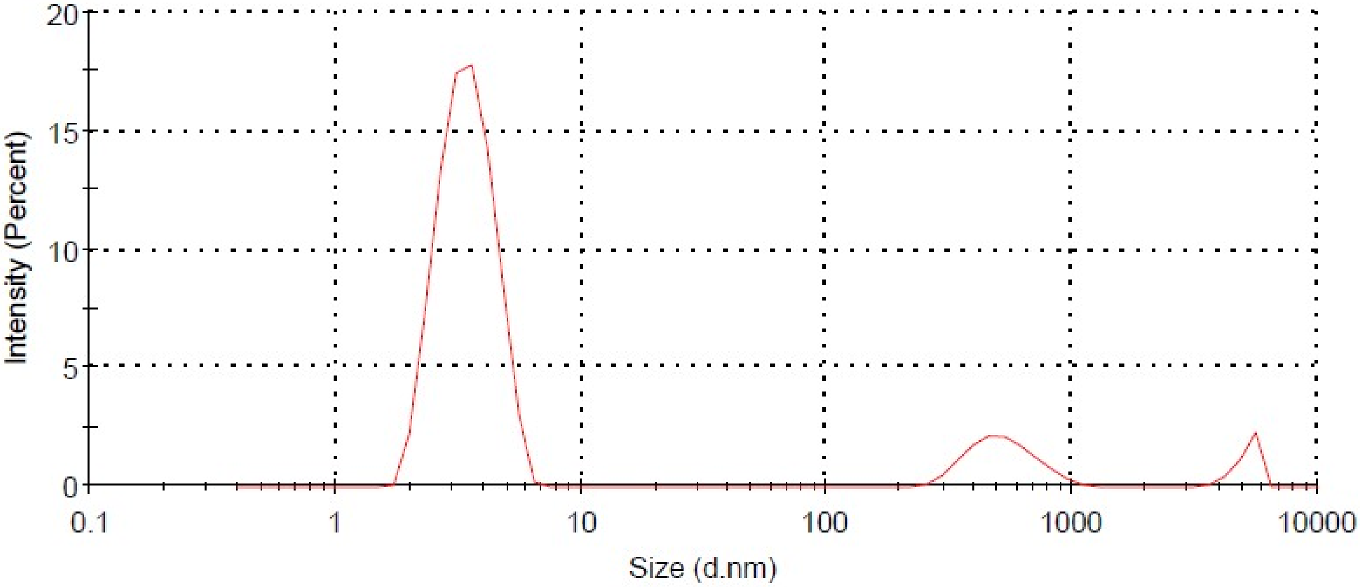

Figure S72. DLS average measurement of **C1** in THF (67%) / H_2O (33%)

Table S2. DLS measurement of **C1** in THF (47%) / H_2O (53%)

Measurement ID	Measurement name	PdI	Maximum of the distribution in Intensity (nm)	
			Peak 1	Peak 2
1	C153 1	-	818.5	2.864
2	C153 2	-	867.9	2.922
3	C153 3	-	1133	2.894
4	C153 4	-	1100	2.899
5	C153 5	-	936.7	2.909
6	C153 6	-	1151	2.800
Average ±SD (%)		-	1001 ± 145 (94.4)	2.88 ± 0.04 (5.3)

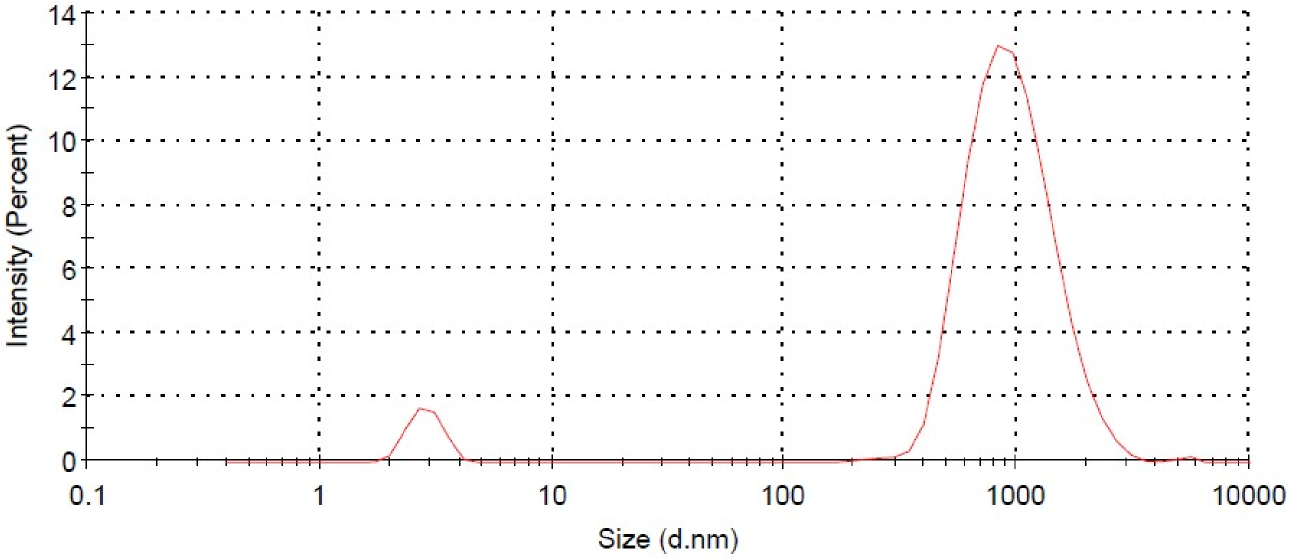

Figure S73. DLS average measurement of **C1** in THF (47%) / H_2O (53%)

Table S3. DLS measurement of **C1** in THF (33%) / H_2O (67%)

Measurement ID	Measurement name	PdI (±SD)	Maximum of the distribution in Intensity (nm)
			Peak 1
1	C167 1	0.073	153.0
2	C167 2	0.073	154.0
3	C167 3	0.024	149.3
4	C167 4	0.067	152.0
5	C167 5	0.061	153.5
6	C167 6	0.051	155.4
Average ±SD (%)		0.06 ± 0.02	152 ± 2 (100)

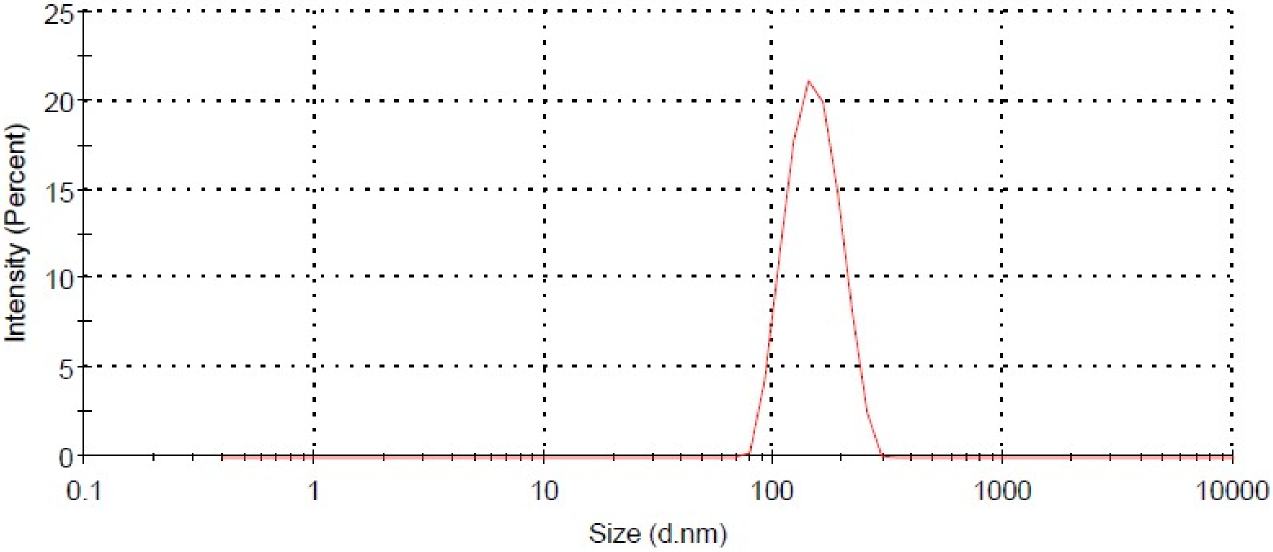

Figure S74. DLS average measurement of **C1** in THF (33%) / H_2O (67%)

Table S4. DLS measurement of **C1** in THF (18%) / H_2O (82%)

Measurement ID	Measurement name	PdI	Maximum of the distribution in Intensity (nm)	
			Peak 1	Peak 2
1	C182 1	0.231	162.2	5243
2	C182 2	0.220	166.2	4630
3	C182 3	0.236	162.8	4377
4	C182 4	0.250	167.5	4539
5	C182 5	0.234	173.7	4730
6	C182 6	0.229	156.3	4602
Average ±SD (%)		0.23 ± 0.01	165 ± 6 (96.9)	4687 ± 296 (3.1)

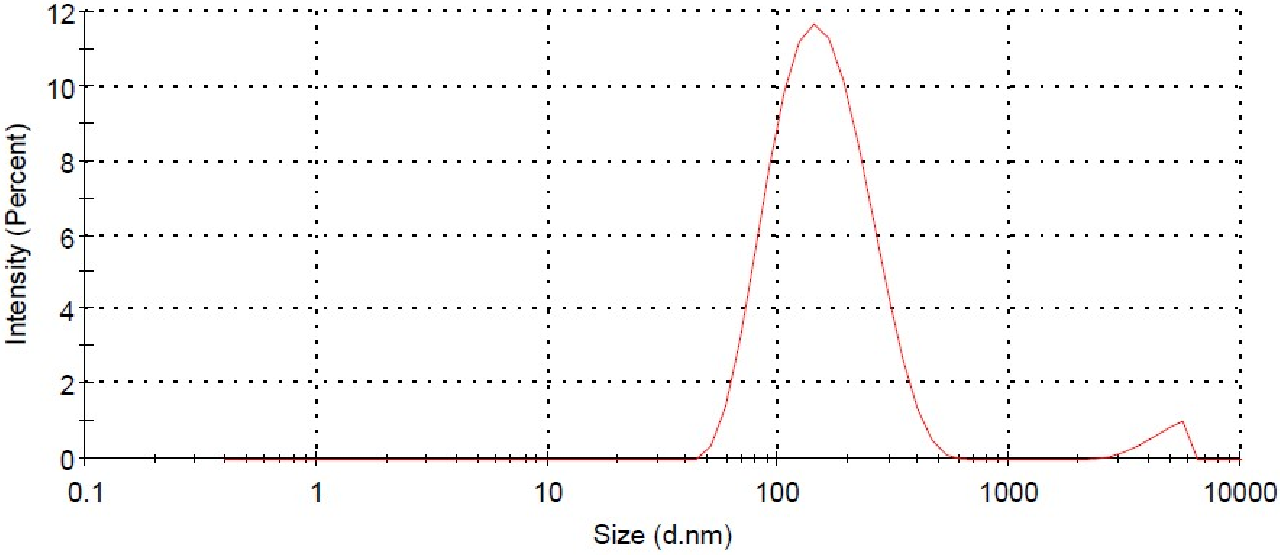

Figure S75. DLS average measurement of **C1** in THF (18%) / H_2O (82%)

Table S5. DLS measurement of **C1** in THF (5%) / H_2O (95%)

Measurement ID	Measurement name	PdI (±SD)	Maximum of the distribution in Intensity (nm)
			Peak 1
1	C195 1	0.087	166.0
2	C195 2	0.081	164.6
3	C195 3	0.106	164.4
4	C195 4	0.119	170.2
5	C195 5	0.117	168.3
6	C195 6	0.104	165.2
Average ±SD (%)		0.10 ± 0.01	166 ± 2 (100)

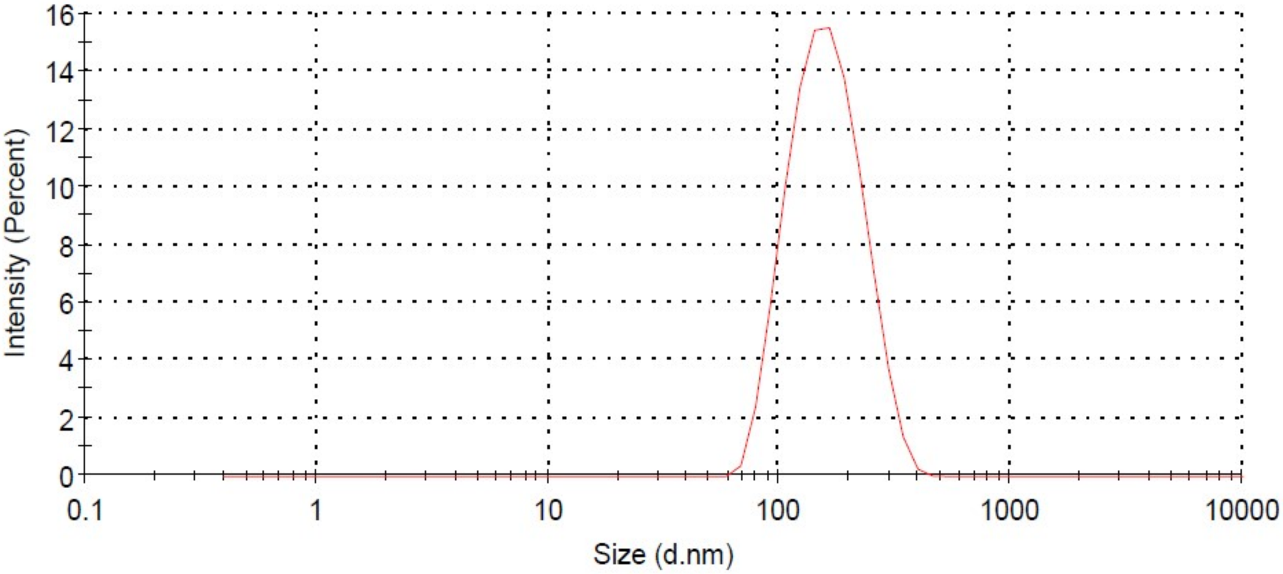

Figure S76. DLS average measurement of **C1** in THF (5%) / H_2O (95%)

Table S6. DLS measurement of **C2** in THF (67%) / H_2O (33%)

Measurement ID	Measurement name	PdI	Maximum of the distribution in Intensity (nm)		
			Peak 1	Peak 2	Peak 3
1	C233 1	-	3.310	394.9	5447
2	C233 2	-	3.411	325.0	5511
3	C233 3	-	3.392	357.5	5451
4	C233 4	-	3.452	364.6	5372
5	C233 5	-	3.510	363.0	5346
6	C233 6	-	3.464	281.1	5560
Average ±SD (%)		-	3.42 ± 0.07 (78.4)	348 ± 39 (18.7)	5448 ± 81 (2.9)

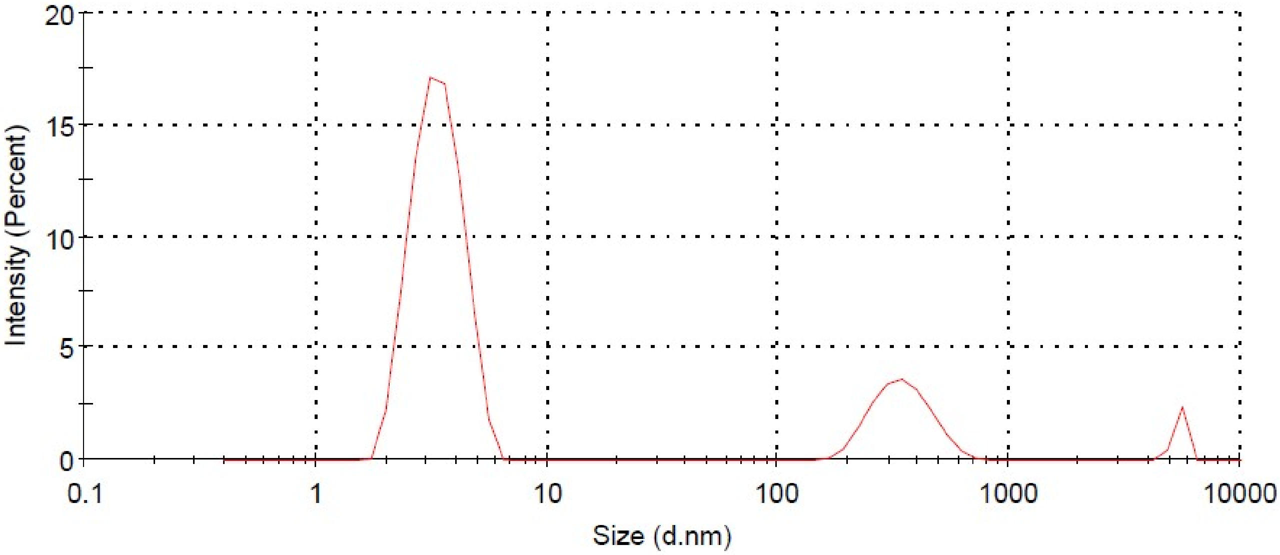

Figure S77. DLS average measurement of **C2** in THF (67%) / H_2O (33%)

Table S7. DLS measurement of **C2** in THF (47%) / H_2O (53%)

Measurement ID	Measurement name	PdI	Maximum of the distribution in Intensity (nm)	
			Peak 1	Peak 2
1	C253 1	0.317	881.1	0
2	C253 2	0.274	947.1	0
3	C253 3	0.326	976.5	5560
4	C253 4	0.299	1001	5421
5	C253 5	0.336	948.9	5560
6	C253 6	0.345	911.2	0
Average ±SD (%)		0.32 ± 0.03	944 ± 43 (99)	5514 ± 66 (1)

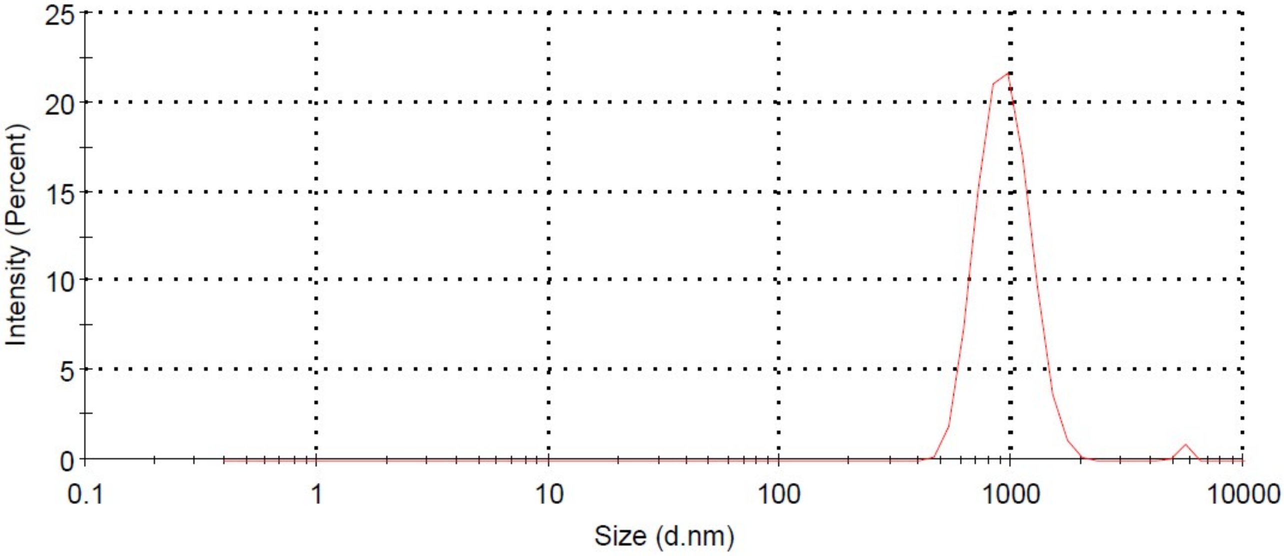

Figure S78. DLS average measurement of **C2** in THF (47%) / H_2O (53%)

Table S8. DLS measurement of **C2** in THF (33%) / H_2O (67%)

Measurement ID	Measurement name	PdI (±SD)	Maximum of the distribution in Intensity (nm)		
			Peak 1	Peak 2	Peak 3
1	C267 1	0.546	105.0	481.1	5560
2	C267 2	0.625	99.38	450.6	5560
3	C267 3	0.492	102.7	444.3	0
4	C267 4	0.525	125.6	517.3	0
5	C267 5	0.521	117.4	460.8	5522
6	C267 6	0.496	108.0	465.7	0
Average ±SD (%)		0.53 ± 0.05	110 ± 10 (16.6)	470 ± 26 (82.6)	5547 ± 20 (0.8)

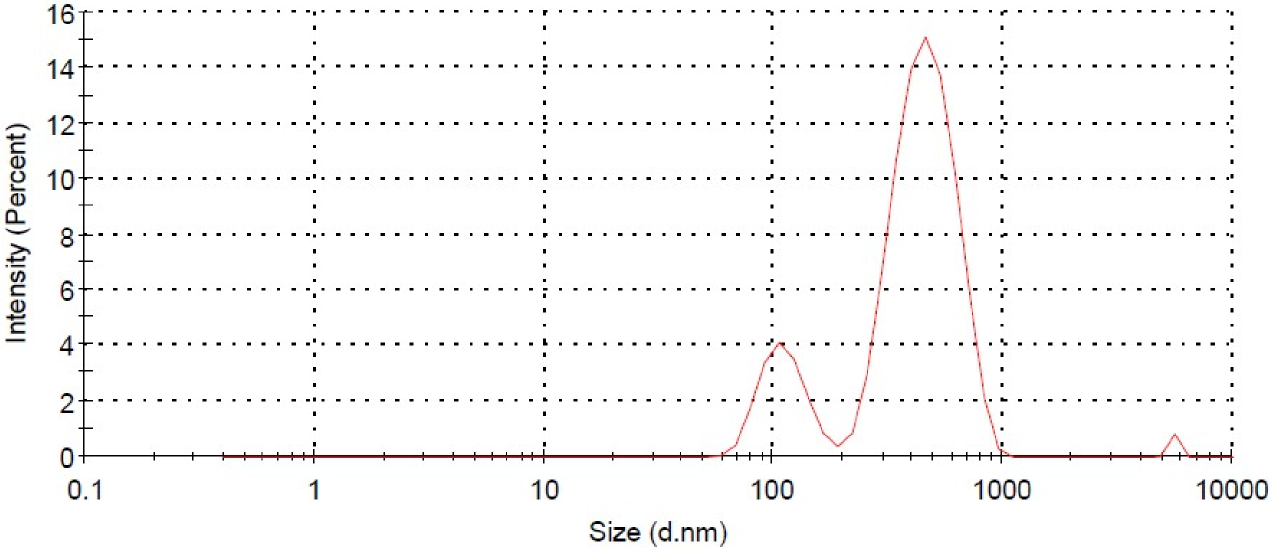

Figure S79. DLS average measurement of **C2** in THF (33%) / H_2O (67%)

Table S9. DLS measurement of **C2** in THF (18%) / H_2O (82%)

Measurement ID	Measurement name	PdI (±SD)	Maximum of the distribution in Intensity (nm)
			Peak 1
1	C282 1	0.159	139.4
2	C282 2	0.147	141.1
3	C282 3	0.148	147.9
4	C282 4	0.141	143.6
5	C282 5	0.121	143.6
6	C282 6	0.125	145.4
Average ±SD (%)		0.14 ± 0.01	143 ± 3 (100)

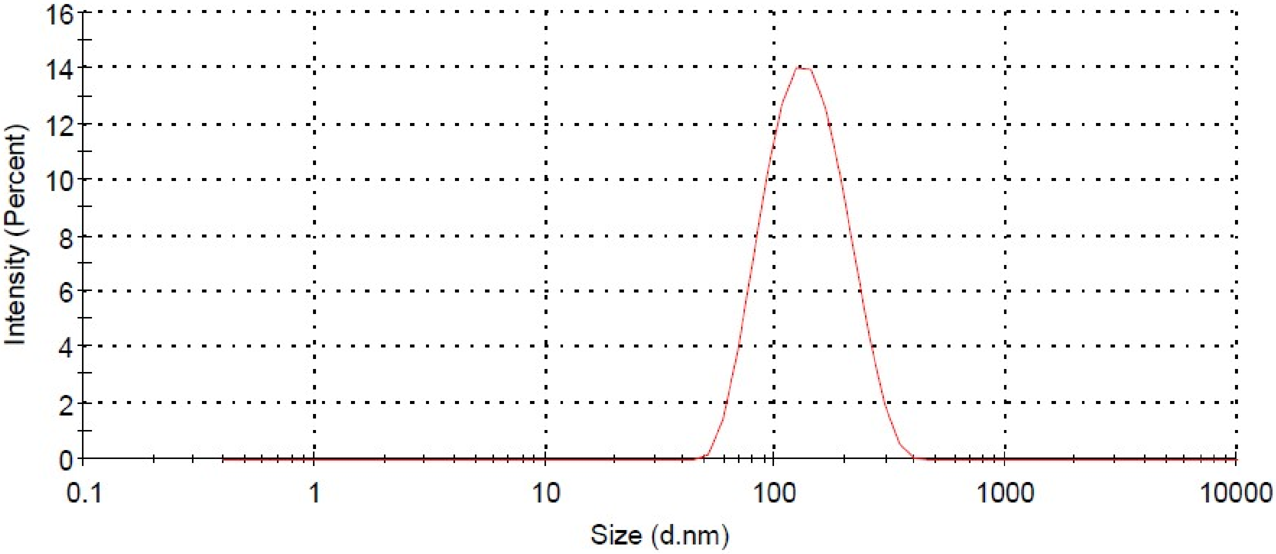

Figure S80. DLS average measurement of **C2** in THF (18%) / H_2O (82%)

Table S10. DLS measurement of **C2** in THF (5%) / H_2O (95%)

Measurement ID	Measurement name	PdI (±SD)	Maximum of the distribution in Intensity (nm)
			Peak 1
1	C295 1	0.115	140.2
2	C295 2	0.120	141.8
3	C295 3	0.111	138.9
4	C295 4	0.117	139.7
5	C295 5	0.112	138.3
6	C295 6	0.101	139.3
Average ±SD (%)		0.113 ± 0.007	140 ± 1 (100)

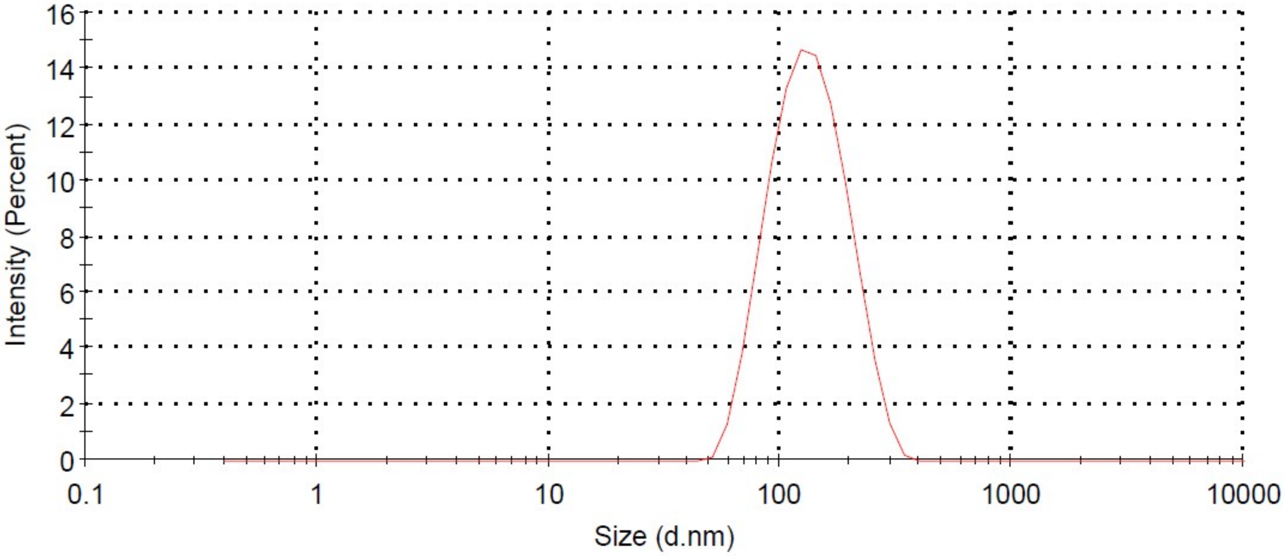

Figure S81. DLS average measurement of **C2** in THF (5%) / H_2O (95%)

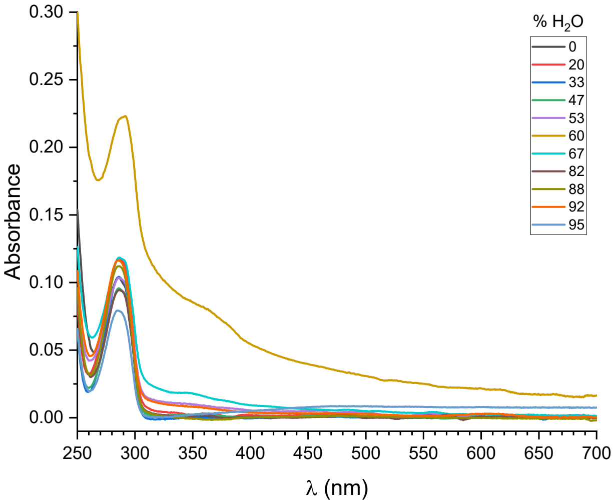

Figure S82. Absorbance spectra of **C1** used to measure emission spectra.

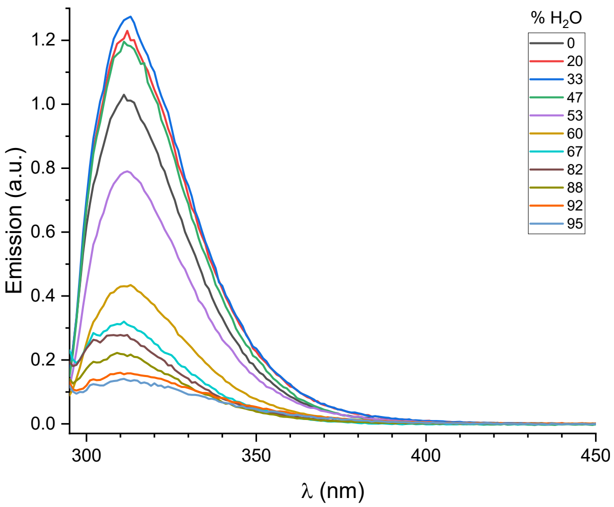

Figure S83. Emission spectra of **C1**.

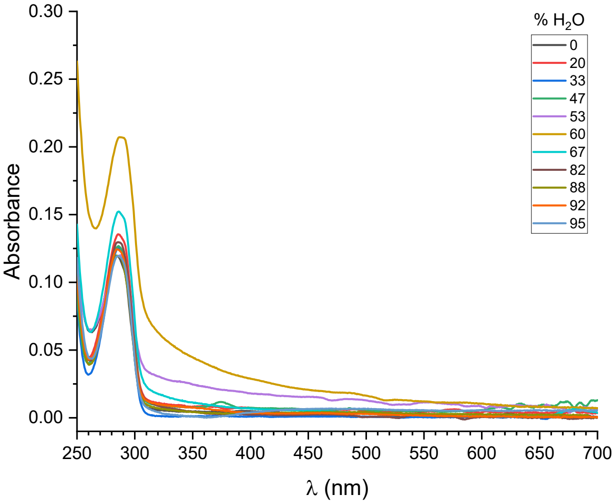

Figure S84. Absorbance spectra of **C2** used to measure emission spectra.

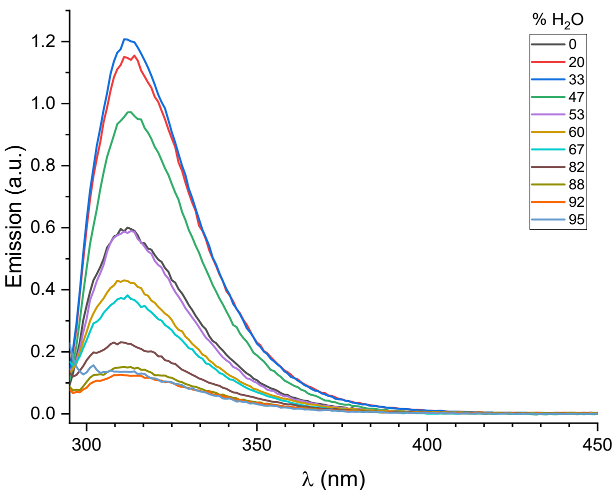

Figure S85. Emission spectra of **C2**.

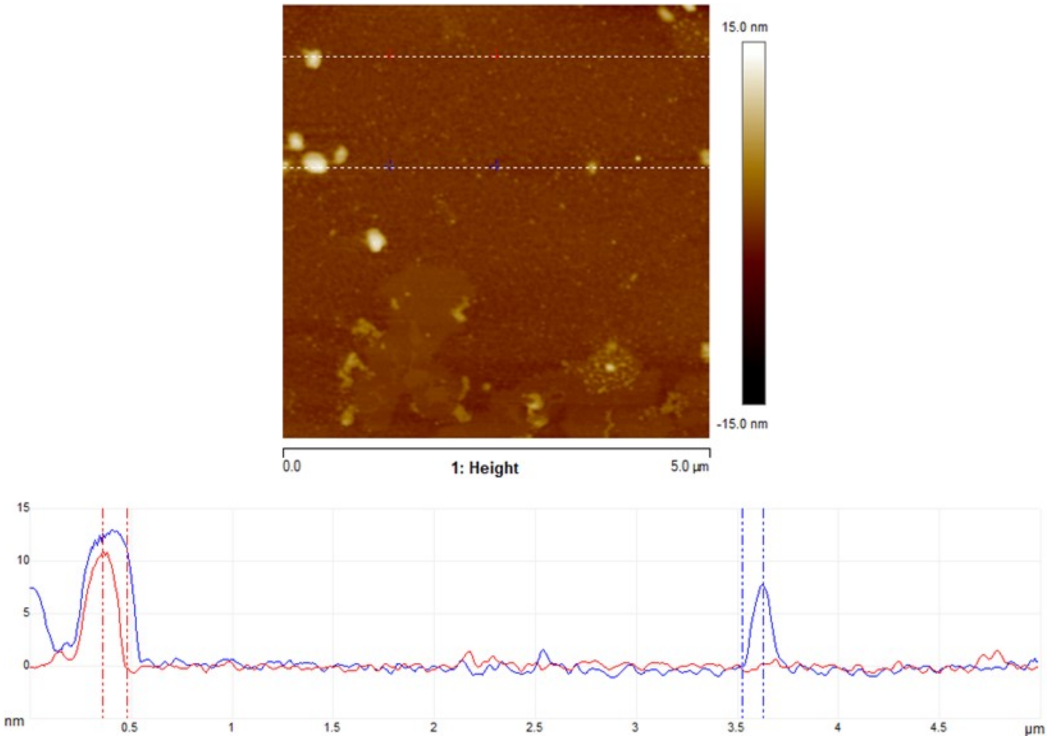

Figure S86. AFM images of **C1** in THF (47%) / H_2O (53%).

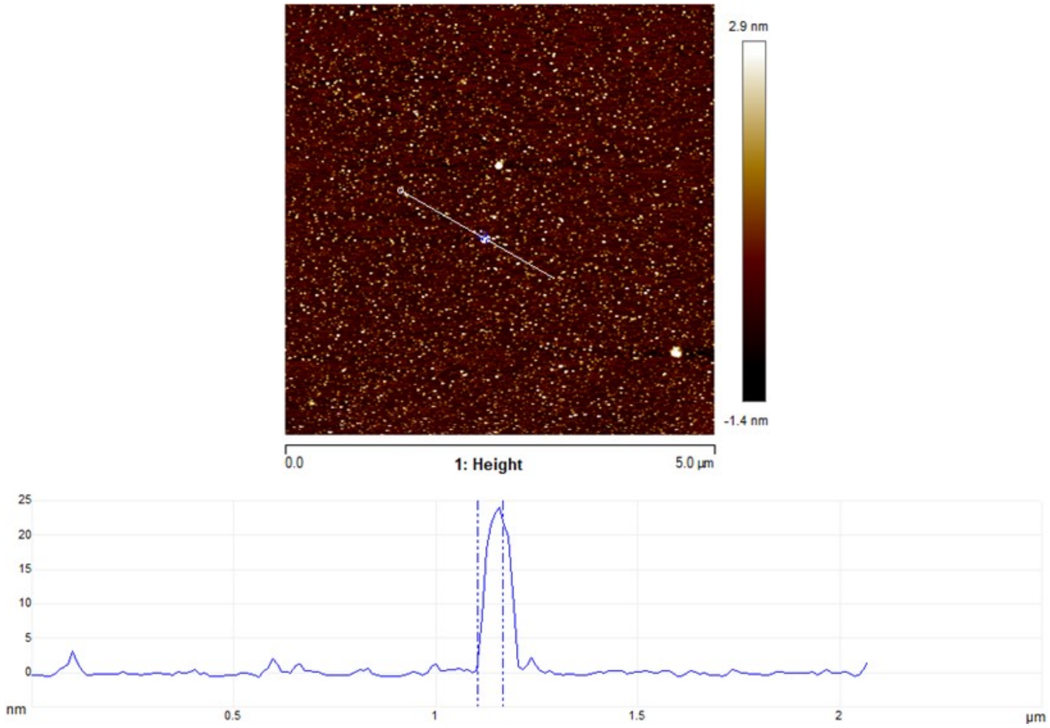

Figure S87. AFM images of **C1** in THF (5%) / H_2O (95%).

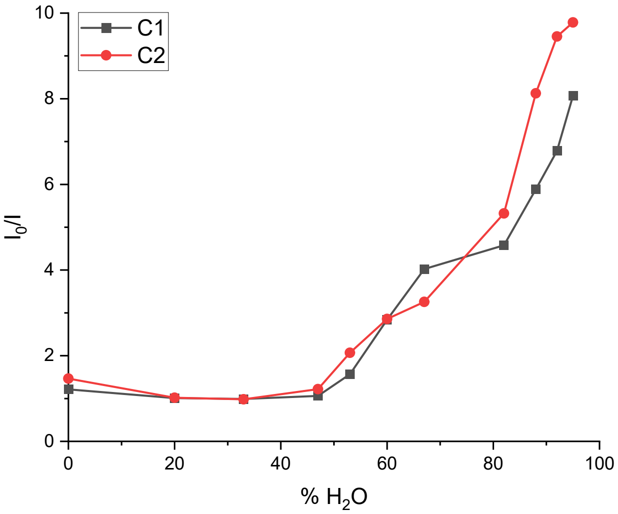

Figure S88. Ratio between relative fluorescence intensities at the maximum of emission spectra, I_0/I, as a function of % H_2O for **C1** and **C2**.

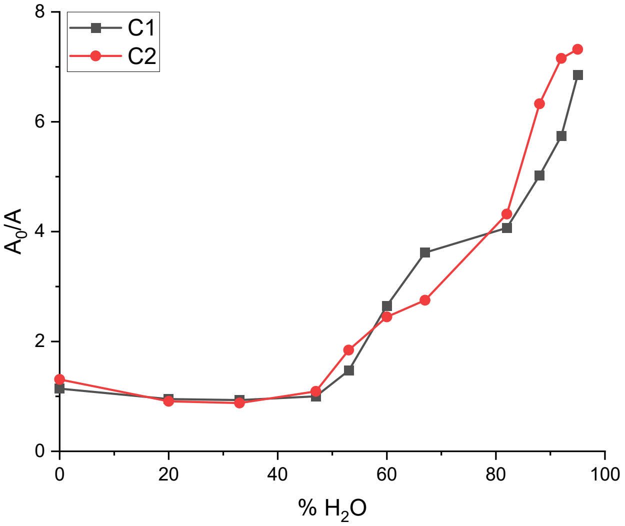

Figure S89. Ratio between relative fluorescence areas values, A_0/A, as a function of % H_2O for **C1** and **C2**.